

**BREAKDOWNS BEHAVIOUR OF GAS-FILLED  
CYLINDRICALLY SHAPED CAPACITOR**

by

MOHD AFNAN BIN OTHMAN

Dissertation report submitted in partial fulfilment of  
the requirements for the  
Bachelor of Engineering (Hons)  
(Electrical & Electronics Engineering)

DECEMBER 2010

Universiti Teknologi PETRONAS  
Bandar Seri Iskandar  
31750 Tronoh  
Perak Darul Ridzuan

## **CERTIFICATION OF APPROVAL**

### **BREAKDOWNS BEHAVIOUR OF GAS-FILLED CYLINDRICALLY SHAPED CAPACITOR**

by

Mohd Afnan bin Othman

A project dissertation submitted to the  
Electrical & Electronics Engineering Programme  
Universiti Teknologi PETRONAS  
in partial fulfilment of the requirement for the  
Bachelor of Engineering (Hons)  
(Electrical & Electronics Engineering)

Approved:

---

Dr Zainal Arif Burhanudin  
Project Supervisor

UNIVERSITI TEKNOLOGI PETRONAS  
TRONOH, PERAK

December 2010

## **CERTIFICATION OF ORIGINALITY**

This is to certify that I am responsible for the work submitted in this project, that the original work is my own except as specified in the references and acknowledgements, and that the original work contained herein have not been undertaken or done by unspecified sources or persons.

---

Mohd Afnan bin Othman

## ABSTRACT

This project is about optimizing the shape of the gas-filled cylindrical-shaped ionization gas sensor in order to improve its performance. Currently available ionization gas sensors may not be well optimized in terms of their sensitivity. In this project, an ionization gas sensor with different electrodes spacing will be simulated to investigate the behavior of the sensor for various phases. The curvature of the electrodes will be varied and the breakdown voltage will be determined from the result obtained. The main activity of this project is simulating the gas sensor using XPDC1 code. XPDC1 code is used to simulate the plasma discharge in a cylindrical-shaped ionization gas sensor. The result of the simulation is being analyzed focusing on the electrons density during breakdown and breakdown voltage. It is found that the electron density is decreased initially due to the recombination and other losses factor. Electrons density then increased after a period of time due to the ionization processes and lead to the sensor breakdown. Electrons density observed during breakdown varied for different setting of electrodes. Higher numbers of electrons are observed during sensor breakdown with 0.09m electrodes spacing and lead to a longer time taken for the sensor to breakdown. At 1.0 Torr, fastest response to breakdown is when electrodes spacing is set to be 0.05m. However, when pressure is set to be higher, the result obtained is different due to the decrease in mobility and diffusion processes. At 1000 Torr, fastest response to breakdown is when electrodes spacing is set to be 0.09m. Breakdown voltage for various electrodes spacing is calculated and it is dependent on the product of electrodes spacing and pressure. This project will be able to optimize the sensitivity of the sensor with regard to its curvature.

## **ACKNOWLEDGEMENTS**

I would like to take the opportunity to express my utmost gratitude to the individual that have taken the time and effort to assist me in completing the project. Without the cooperation of these individuals, no doubt I would have faced some complications through out the course.

First and foremost my utmost gratitude goes to my supervisor, Dr Zainal Arif bin Burhanudin for the dedication of his time and effort, relentlessly teaching and guiding me despite his other obligations. Without his guidance and patience, I would not be succeeded to complete the project. I also would like to express my appreciation to Mr Salman Mahmood for his willingness to assist me to understand the project. Many thanks to the Electrical and Electronic Engineering Department for providing me with all the utilities and information required to begin the project.

My appreciation also extended to my family and friends who encouraged and supported me throughout the completion of this project. Not to forget, special thanks to all individuals that has helped me in any way, but whose name is not mentioned here, I thank you all.

## TABLE OF CONTENTS

<b>ABSTRACT</b>		iv
<b>LIST OF FIGURES</b>		viii
<b>LIST OF TABLES</b>		x
<b>CHAPTER 1:</b>	<b>INTRODUCTION</b>	1
1.1	Background of Study	1
1.2	Problem Statement	8
1.3	Objectives	8
1.4	Scope of Study	9
<b>CHAPTER 2:</b>	<b>LITERATURE REVIEW</b>	10
2.1	Theory	10
2.2	Ionization	10
2.2.1	<i>Ionization by collision.</i>	11
2.2.2	<i>Secondary ionization</i>	13
2.3	Recombination	15
2.4	Breakdown Voltage	16
2.5	Paschen's Curve	17
2.6	XPDC1 code	20
<b>CHAPTER 3:</b>	<b>METHODOLOGY</b>	21
3.1	Procedure Identification	21
3.2	Tools and Equipments	22
<b>CHAPTER 4:</b>	<b>RESULTS AND DISCUSSION</b>	23
4.1	Result	23

	4.1.1	<i>Experiment 1: <math>r_0</math> Fixed, <math>r_1</math> Varied</i>	24
	4.1.2	<i>Experiment 2: <math>r_0</math> Varied, <math>r_1</math> Fixed.</i>	35
	4.1.3	<i>Experiment 3: Pressure variation</i>	46
4.2		Discussion	52
	4.2.1	<i>Electrons loss mechanism</i>	52
	4.2.2	<i>2 Electrons production</i>	56
	4.2.3	<i>The curvature effect</i>	56
	4.2.4	<i>Electron mobility</i>	58
	4.2.5	<i>Sheath formation</i>	58
	4.2.6	<i>Sensor breakdown</i>	60
	4.2.7	<i>Breakdown voltage</i>	61
	4.2.8	<i>Effects of pressure</i>	65
<b>CHAPTER 5:</b>		<b>CONCLUSION AND RECOMMENDATION</b>	68
	5.1	Conclusion	68
	5.2	Recommendation	69
<b>REFERENCES</b>			70
<b>APPENDICES</b>			73
		APPENDIX A	74
		APPENDIX B	75
		APPENDIX C	76

## LIST OF FIGURES

Figure 1: Smoke sensor . . . . .	1
Figure 2: Ionization chamber and electrical horn . . . . .	2
Figure 3: Gas slot for gases to flow into ionization chamber . . . . .	3
Figure 4: MEMS-based gas sensor . . . . .	4
Figure 5: Semiconductor metal-oxide gas sensor . . . . .	5
Figure 6: Model of inter-grain potential barrier (in the absence of gases)	6
Figure 7: Model of inter-grain potential barrier (in the presence of gases)	6
Figure 8: Illustration of ionization process . . . . .	11
Figure 9: Parallel-plane ionization gas sensor . . . . .	11
Figure 10: Ionization by electron collides with neutral atom . . . . .	12
Figure 11: Ionization by electron impact . . . . .	13
Figure 12: Positive ion collides with cathode surface . . . . .	14
Figure 13: Paschen's Curve . . . . .	19
Figure 14: Cylindrical shape ionization gas sensor . . . . .	20
Figure 15: Work flow for completing the simulation . . . . .	21
Figure 16: Average density versus time . . . . .	26
Figure 17: Density versus electrodes spacing at $t=0$ s . . . . .	28
Figure 18: Arrangement for cathode and anode. . . . .	29
Figure 19: Electrons and Argon charges between electrodes. . . . .	29
Figure 20: Density versus electrodes spacing at $t=7E-9$ s . . . . .	30
Figure 21: Density versus electrodes spacing at breakdown . . . . .	32
Figure 22: Density versus electrodes spacing at $t=2.7E-6$ s . . . . .	33
Figure 23: Average density versus time . . . . .	37



Figure 24: Density versus electrodes spacing at $t=0$ s	39
Figure 25: Density versus electrodes spacing at $t=7E-9$ s	41
Figure 26: Density versus electrodes spacing during breakdown	43
Figure 27: Density versus electrodes spacing at $t=2.7E-6$ s	44
Figure 28: Result obtained during breakdown for $r_0=0.01m$ and $r_1=0.06m$	46
Figure 29: Result obtained during breakdown for $r_0=0.01m$ and $r_1=0.08m$	47
Figure 30: Result obtained during breakdown for $r_0=0.01m$ and $r_1=0.1m$ .	48
Figure 31: Result obtained during breakdown for $r_0=0.03m$ and $r_1=0.1m$ .	49
Figure 32: Result obtained during breakdown for $r_0=0.05m$ and $r_1=0.1m$	50
Figure 33: Sheath formed at electrodes wall	59
Figure 34: Breakdown voltage Versus Pressure time distance product	67

## LIST OF TABLES

Table 1: Ionization energies for various inert gases . . . .	15
Table 2: Work function for various metals . . . . .	15
Table 3: The values of $C_1$ and $C_2$ for the analytical model of Townsend's first ionization coefficient . . . . .	17
Table 4: Minimum breakdown voltage for various gases . . . .	19
Table 5: Electrodes setting for Experiment 1 . . . . .	25
Table 6: Electrodes setting for Experiment 2 . . . . .	36
Table 7: Time taken for sensor to breakdown . . . . .	51
Table 8: Electrons density observed during breakdown . . . .	51
Table 9: Comparison between Experiment 1 and Experiment 2 . .	57
Table 10: Minimum breakdown voltage for various electrodes spacing (Experiment 1, $r_0$ fixed at 0.01m) . . . . .	63
Table 11: Minimum breakdown voltage for various electrodes spacing (Experiment 2, $r_1$ fixed at 0.1m) . . . . .	64
Table 12: Minimum breakdown voltage for various pressures. . . .	66

# CHAPTER 1

## INTRODUCTION

### 1.1 Background of Study

Gas sensor is a device which detects the presence of various gases within an area. This type of equipment is used to detect a gas leak and interface with a control system so alarm system will be triggered and preventive actions can be taken by automatically shut down a process. It is usually as a part of safety system in the plant or other hazardous industry which involve gas emissions such as petrochemical plant. In this industry, monitoring and detection of gases play an important role for the safety of the workers and environment [1].

For instance, smoke sensor is one of the gas sensing devices which will sense the existence of smoke in a confined area such as house and office. Figure 1 below shows the commercial smoker sensor. Various gases such as carbon monoxide and carbon dioxide can be found in smoke produce by flame, therefore, when fire happened, the sensor will detect the smoke produced and electronic alarm built inside the sensor will be triggered to alert people nearby [1].



Figure 1: Smoke sensor

Gas sensors basically using the ionization principal to operate and because of this principal, gas sensors are also known as ionization gas sensor. There are several other techniques and principals in sensing gas presence such as catalytic gas sensors, infrared gas sensors, semiconductor metal-oxide gas sensors, absorption-based gas sensors, and MEMS-based gas sensors. Although the principles and techniques used for gas sensors are different, but they still being used for the same purpose.

Ionization gas sensors operate based on fingerprinting ionization characteristics of different gases. It is called ionization gas sensor because it involved ionization process which is a process of energizing an electron from a gas molecule with the simultaneous production of a positive ion [2].

Figure 2 below shows an ionization smoke sensor using an ionization chamber which contains ionization source [1]. When voltage applied to the electrodes inside the chamber, the ionization source will gain energy and at certain period of time the energy obtained is sufficient to break the atomic bond of the gas and breakdown occurs. When breakdown occurred, the gas which is an insulator at the beginning has become a conductor and conduct electricity. At this point, the electrical circuit of the electronic alarm system is completed and the electrical horn will be triggered.

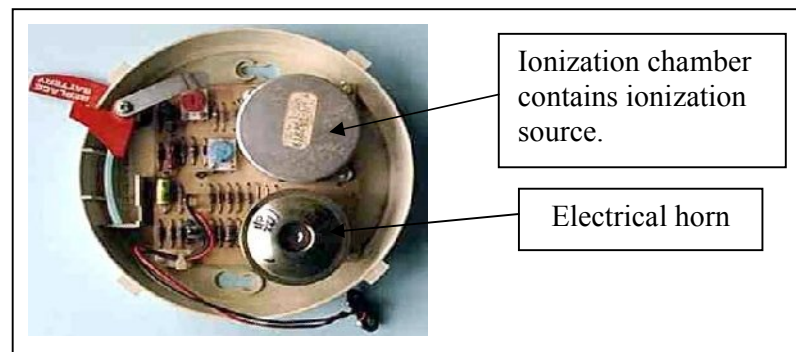


Figure 2: Ionization chamber and electrical horn

Figure 3 below shows that the ionization chamber has slots or openings. The slots is used for gases to flow into the chamber and mixed with the ionization source [1]. When a mixture of gases passed through two electrodes, it will be ionized when it reach a certain period of time and caused breakdown [3].

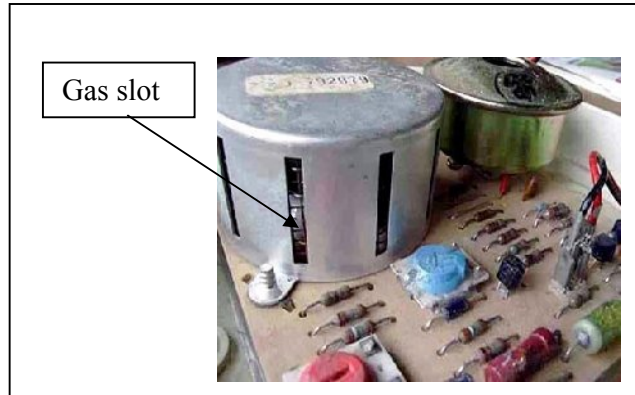


Figure 3: Gas slot for gases to flow into ionization chamber

Other type of gas sensor is MEMS-based or Micro-Electro-Mechanical Systems gas sensor. It is a sensing device manufactured using MEMS technology. MEMS is the integration of mechanical elements, sensors, actuators, and electronics on a common silicon substrate through microfabrication technology. While the electronics are fabricated using integrated circuit (IC) process sequences, the micromechanical components are fabricated using compatible "micromachining" processes that selectively carve away parts of the silicon wafer or add new structural layers to form the mechanical and electromechanical devices. Figure 4 shows the overview of the MEMS-based sensor and the MEMS sensor itself [4].

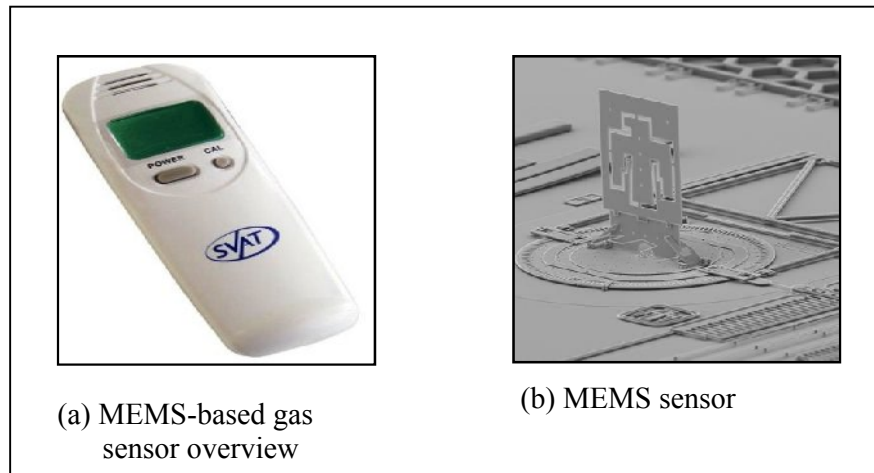


Figure 4: MEMS-based gas sensor

Figure 4 shows MEMS-based sensor used to gather information from the environment through measuring mechanical, thermal, biological, chemical, optical, and magnetic phenomena. The whole sensor system is controlled by microelectronic integrated circuits in the MEMS sensor. The electronics then process the information derived from the sensors and through some decision making capability direct the actuators to respond by moving, positioning, regulating, pumping, and filtering, thereby controlling the environment for some desired outcome or purpose [4].

Since MEMS devices are manufactured using batch fabrication techniques similar to those used for integrated circuits, they have unique levels of functionality, reliability, and complexity.

MEMS-based gas sensor usually used by Environment, Health and Safety (EHS) Inspector when they are inspecting the hazardous industry such as petrochemical plant to ensure the industry is complying with the law in terms of gas emission and the safe workplace.

In gas sensing industry, semiconductor metal-oxide gas sensors stand out among other sensors. For instance,  $\text{SnO}_2$  based sensors are the leading solid-state gas sensors for domestic, commercial and industrial application. The sensor is shown in Figure 5 below.



Figure 5: Semiconductor metal-oxide gas sensor

The principle operation of this type of sensor is quite simple as compared to other gas sensing devices. Taking  $\text{SnO}_2$  based gas sensor as an example, when a metal oxide crystal such as  $\text{SnO}_2$  is heated at a certain high temperature in air, oxygen is adsorbed on the crystal surface with a negative charge. Then, donor electrons in the crystal surface are transferred to the adsorbed oxygen. The process results in leaving positive charges in a space charge layer. Thus, surface potential is formed to serve as a potential barrier against electron flow [5,6].

Inside the sensor, electric current flows through the conjunction parts also known as grain boundary of  $\text{SnO}_2$  micro crystals. At grain boundaries, the adsorbed oxygen forms a potential barrier which prevents carriers from moving freely. The electrical resistance of the sensor is attributed to this potential barrier [5,6].

In the presence of a deoxidizing gas which is the gas from surrounding area, the surface density of the negatively charged oxygen decreases, so the barrier height in the grain boundary is reduced. The reduced barrier height decreases sensor resistance and increasing conductivity of the material, thus, the material will conduct electricity and trigger the alarm [5]. The operation principle of the sensor can simply be understood by referring to Figure 6 and Figure 7 below.

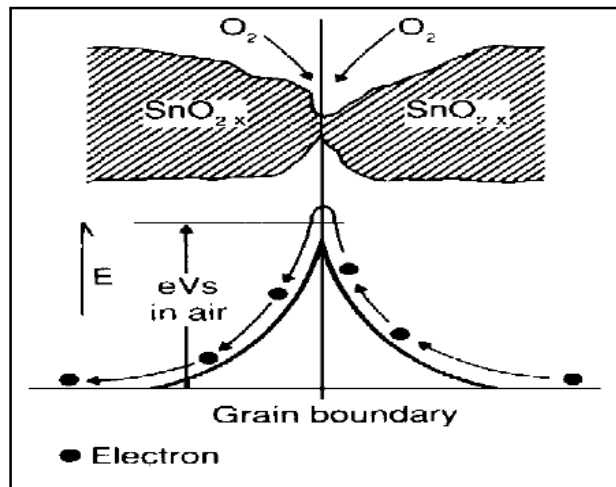


Figure 6: Model of inter-grain potential barrier (in the absence of gases)

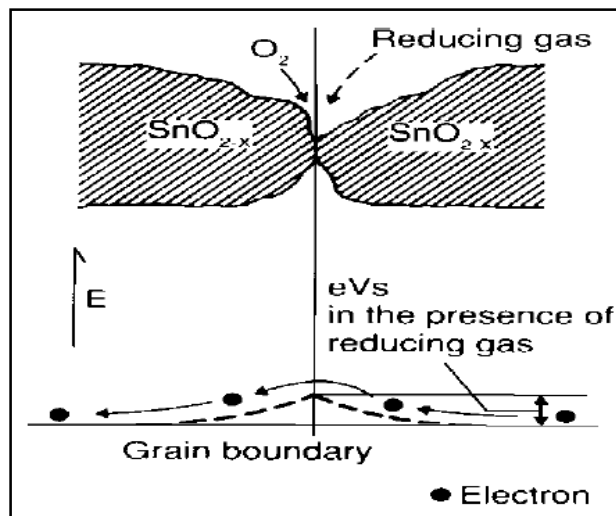


Figure 7: Model of inter-grain potential barrier (in the presence of gases)



The advantage of semiconductor metal-oxide gas sensor compared to other types of gas sensor is the cost for manufacturing it. Semiconductor metal-oxide gas sensor is low cost and easy to produce. This is the main reason why this type of sensor is the leader in gas sensing devices industry. It also has compact size and rigid construction. This type of sensor involves simple measuring electronics compared to other sensors which are more complex.

However, semiconductor metal-oxide gas sensor suffers mostly from a lack of gas selectivity. For instance, the most commonly used oxide,  $\text{SnO}_2$ , can be sensitized to different gases by judicious choice of operating temperature, microstructural modification, and by the use of dopants and catalysts [6]. Even though the performance is improved, but it will have some effect on the size and the production cost for the sensor.

Compared to absorption-based gas sensors, ionization gas sensor is not limited by the electrophilicity or absorption energy of gases. Instead, ionization-based sensors are sensitive to the gaseous ionization and drift property, which gives them many properties such as faster response, quicker recovery, hard to be poisoned, and sensitive to many gases [19].

Ionization gas sensor uses simple mechanism for gas detection and makes it easy to manipulate the sensor for optimization purposes compared to MEMS-based gas sensor which used complex and advanced electronic equipment for gas detection. Thus, it makes it difficult to manipulate MEMS-based gas sensor. Furthermore, ionization gas sensor is cheaper than MEMS-based gas sensor. MEMS-based gas sensor is expensive since it involved advanced electronic equipments and complex circuit construction for its operation [4]. In addition, this sensor is appropriate for EHS personnel and not applicable to be used as a part of safety system in hazardous industry.

Based on the preliminary study being done, ionization gas sensor is preferred to be the main concern in this project. This sensor will be further studied in order to investigate the processes involved and to improve the sensor performance.

## **1.2 Problem Statement**

Currently available ionization gas sensor may not be well optimized. The sensitivity of the gas sensor can be improved further by studying its breakdown behaviour and optimizing the shape of the sensor.

The sensitivity of ionization gas sensor depends on the spacing of the electrodes. The radius of inner and outer electrodes will affect the time taken for the sensor to breakdown. The sensitivity of the sensor is decreased if the time taken for breakdown to occur is longer.

Breakdown potential or breakdown voltage of a cylindrical-shaped ionization gas sensor is the potential difference measured between two electrodes when the sensor conducts electricity and it is dependent on the distance between two electrodes. Breakdown potential will be higher if the distance between two electrodes is increased.

## **1.3 Objective**

The objective of this project is

- To investigate the curvature effect of cylindrically-shaped ionization gas sensor on the breakdown voltage and electrons density between two electrodes.
- To optimize the sensitivity of ionization gas sensor by optimizing the shape of the sensor.

#### **1.4 Scope of Study**

This project will use Cylindrical Plasma Device 1 Dimensional Bounded Electrostatic Code (XPDC1) and Parallel-plane Plasma Device 1 Dimensional Bounded Electrostatic Code (XPDP1) for simulation purposes. The simulation codes are used to simulate the real-time running processes of the gas sensor.

For the first part of the project, XPDP1 code will be used for the purpose of understanding and familiarizing with the simulation. The simulation is conducted using XPDC1 code to acquire data and result in order to analyze the gas sensor performance.

The data obtained from the simulation will determine the performance of the sensor based on the parameters being set in the input file. This project is expected to be completed by the end of the semester.

## **CHAPTER 2**

### **LITERATURE REVIEW**

#### **2.1 Theory**

The simulation of breakdown behaviour of an ionization gas sensor is a task of obtaining a model of an ionization gas sensor with the optimum sensitivity and selectivity by manipulating the curvature of the cylindrical-shaped ionization gas sensor and keeping the atmosphere pressure and distances between two electrodes constant. The understanding of the gas ionization concept and the breakdown voltage of gas is essential in this project. Furthermore, the processes that take place during the ionization also important in order to analyze the data acquired from the simulation.

#### **2.2 Ionization**

Ionization is the physical process of converting an atom or molecule into an ion by adding or removing charged particles such as electrons or other ions. This process is a process whereby an electron is removed from an atom, molecule, or ion. It is of basic importance to electrical conduction in gases and liquids [8].

In the simplest case, ionization may be thought of as a transition between an initial state consisting of a neutral atom and a final state consisting of a positive ion and a free electron. Figure 8 shows the concept of ionization process.



Figure 8: Illustration of ionization process

For this project, Argon gas has been used as the dielectric medium between two electrodes. A gas in its normal state is almost a perfect insulator. However, when a high voltage is applied between the two electrodes immersed in a gaseous medium, the gas becomes a conductor and an electrical breakdown occurs [9].

The processes that are mainly responsible for the breakdown of a gas are ionization by collision, photoionization, and the secondary ionization processes. In insulating gases, the process of attachment also plays an important role to contribute for a breakdown [9].

### 2.2.1 Ionization by collision

In the process of ionization by collision, a free electron collides with a neutral gas molecule and gives rise to a new electron and a positive ion. For instance, if we consider a low pressure gas column in which an electric field  $E$  is applied across two plane parallel electrodes, any electron starting at the cathode will be accelerated more and more between collisions with other gas molecules during its travel towards the anode [9]. Figure 9 below shows the parallel plane ionization gas sensor that meet the concept explained above.

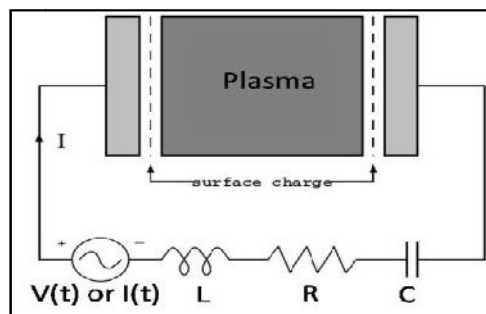


Figure 9: Parallel-plane ionization gas sensor

If the energy ( $\epsilon$ ) gained during this travel between collisions exceeds the ionization potential,  $V_i$ , which is the energy required to dislodge an electron from its atomic shell, then ionization takes place [9]. Direct ionization process is shown in Figure 10 below.

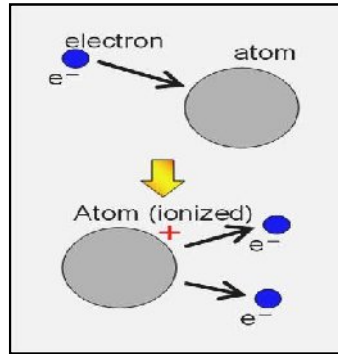
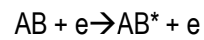
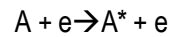


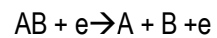
Figure 10: Ionization by electron collides with neutral atom

There are several other types of ionization for atoms and molecules to occur by electron impact besides the direct ionization process such as

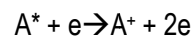
(1) Excitation



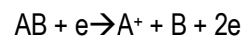
(2) Dissociation



(3) Cumulative ionization



(4) Dissociative ionization



Where  $e$  denotes the electron, A, B or AB denotes the atoms or molecules, and  $A^*$  or  $AB^*$  denotes the excited atom or molecule [10].

### 2.2.2 Secondary ionization

For secondary-ionization process, it is studied from the Townsend theory which indicates the reaction involving electrons in a region with a sufficiently high electric field.

Townsend has specified two coefficients for secondary ionization. The first Townsend coefficient specifies that secondary ionization is by electron impact. The positive ion drifts towards the cathode, while the free electron drifts towards the anode of the particular device. It accelerates in the electric field, gaining sufficient energy such that it frees another electron upon collision with another atom of the medium. The two free electrons then travel together some distance before another collision occurs. The number of electrons travelling towards the anode is multiplied by a factor of two for each collision [15,16].

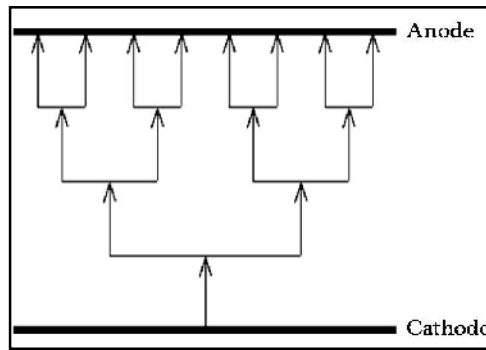


Figure 11: Ionization by electron impact

Townsend's first ionization coefficient is used to determine the number of electrons at a distance  $x$  from the cathode [11].

$$N_e = N_{e0} e^{\alpha_r d} \quad (\text{Equation 2.1})$$

Where  $N_e$  is the number of electrons at a distance  $d$  from cathode,  $N_{e0}$  is the number of electrons emitted at the cathode, and  $\alpha_T$  is the number of ionizing collisions made per unit length which also known as Townsend's first ionization coefficient

The second Townsend coefficient specifies the secondary ionization is caused by positive ion impact with the cathode [15]. Positive ions are drifted towards the cathode and collide with the cathode surface, hence, result in generating electrons. Figure 12 below explains the ionization by positive ion impact with cathode.

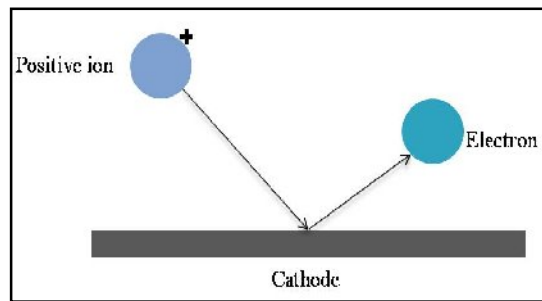


Figure 12: Positive ion collides with cathode surface

Townsend's model for this process involves a second ionization coefficient  $\gamma_T$  to account for secondary emissions of electrons leading to a greater electron density, enhanced ionization. The Townsend's second ionization coefficient can be found from equation 2.2 [12].

$$\gamma_T = (0.016/eV) (I - 2\mathcal{G}) \quad (\text{Equation 2.2})$$

where  $I$  is ionization energy and the work function is  $\mathcal{G}$ . A partial list of ionization energy for various inert gases and work functions for various metals are shown in Table 1 and Table 2 [12].



Table 1: Ionization energies for various inert gases

Element	I (eV)
He	24.587
Ne	21.56
Ar	15.75
Kr	14
Xe	12.13
He	24.587

Table 2: Work function for various metals

Element	$\phi$ (eV)	Element	$\phi$ (eV)	Element	$\phi$ (eV)
Cs	1.95	Al	4.28	C	4.7
K	2.3	Sn	4.28	Si	4.95
Na	2.36	Ta	4.3	Co	4.97
Ba	2.52	Ti	4.33	Ni	5.15
U	3.47	Cr	4.44	Au	5.1
Mn	4.08	Mo	4.49	Pd	5.4
Cd	4.22	Cu	4.51	Pt	5.63
Pb	4.25	W	4.55		
Ag	4.26	Fe	4.6		

### 2.3 Recombination

Charged particles can be neutralized in the gas phase or on solid surface will produce neutral atom or molecules. This can be achieved by combining positive ion with an electron or a positive ion with a negative one. This process is called recombination and classified into ion-ion recombination and ion-electron recombination [10].

For both cases, the vanishing rate of charged particles due to recombination is expressed by

$$\frac{dn}{dt} = \frac{dn_+}{dt} = \frac{dn_-}{dt} = -cn + n_- \quad (\text{Equation 2.3})$$

Where  $n_+$  and  $n_-$  are the densities of particles with positive and negative charge, respectively.  $\alpha$  is called the recombination coefficient. The higher the recombination coefficient, more charged particles is vanished [10].

## 2.4 Breakdown Voltage

Breakdown voltage is the voltage at which an electrical breakdown occurs in a dielectric in this case the Argon gas.

Breakdown occurs when gas is transformed from an insulator to a conductor. In an electrically stressed gas, as the voltage is increased, the free electrons present in the gas gain energy from the electric field. When the applied voltage is increased to such a level that an appreciable number of these electrons are energetically capable of ionizing the gas, the gas makes the transition from an insulator to a conductor [17]. During this circumstance, it is observed that the electron densities are high between two electrodes thus allow the gas to conduct electricity.

The breakdown voltage varies significantly from one gaseous medium to another. It is very low for the rare gases and very high for polyatomic especially electronegative gases such as sulfur hexafluoride (SF<sub>6</sub>) [17].

The breakdown potential depends on the nature, number of charged density, and temperature of the gas. The material, state, and geometry of the electrodes will also affect the breakdown potential [17]. For example, if surface area at the electrodes especially the cathode is large or the presence of conducting particles in the gas is high, it will reduces the breakdown potential because at certain points the electric field is significantly enhanced, increasing the electron energy and thus more ionization take place.

The breakdown occurs in times ranging from milliseconds to nanoseconds, depending on the form of the applied field and the gas density.

## 2.5 Paschen's Curve

Using the Townsend breakdown condition with the primary ionization condition, it result in the relation [11]

$$C_1pd \exp\left(-\frac{C_2pd}{V_b}\right) = \ln\left(1 + \frac{1}{\gamma_T}\right) \quad (\text{Equation 2.4})$$

where the breakdown voltage  $V_b$  is given by

$$V_b = E_b d \quad (\text{Equation 2.5})$$

in a plane geometry. Hence

$$\begin{aligned} V_b &= \frac{C_2pd}{\ln\left[\frac{C_1pd}{\ln(1+1/\gamma_T)}\right]} \quad (\text{Equation 2.6}) \\ &= V_b(pd) \end{aligned}$$

Equation 2.6 is a statement of Paschen's law, that is, the breakdown voltage of a gas depends only on  $pd$  since  $C_1$ ,  $C_2$  and  $\gamma_T$  are fixed for each gas. The values for  $C_1$  and  $C_2$  for the analytical model of the first Townsend ionization coefficient for noble gases is given in the Table 3 using the unit conversions  $1\text{cm}=0.01\text{m}$ , and  $1\text{Torr}=1\text{mm-Hg}=133.3224\text{Pa}$  [11].

Table 3: The values of  $C_1$  and  $C_2$  for the analytical model of Townsend's first ionization coefficient

Gas	$C_1$ ( $\text{m}^{-1}\text{Pa}^{-1}$ )	$C_2$ ( $\text{Vm}^{-1}\text{Pa}^{-1}$ )	$C_1$ ( $\text{cm}^{-1}\text{Torr}^{-1}$ )	$C_2$ ( $\text{Vcm}^{-1}\text{Torr}^{-1}$ )
He	1.37	37.5	1.82	50
Ne	3	75	4	100
Ar	9	150	12	200
Kr	10.9	165	14.5	220
Xe	16.7	233	22.2	310

When the pressure-gap product,  $pd$  is high, the electrons mean free path are short. An electron will collide with many different gas molecules as it travels from the cathode to the anode. The collisions randomizes the electron direction, so the electron is not always being accelerated by the electric field to anode, sometimes it travels back towards the cathode for some time and is decelerated by the field. In this situation, large voltages are required for the electrons to accumulate sufficient energy to ionize gas molecules and produce an electrons avalanche [18].

When the  $pd$  product is small, the electrons mean free path can become long compared to the gap between the electrodes. In this case, the electrons might gain lots of energy, but they often arrive at the anode before getting a chance to bump into a gas molecule and start the avalanche [18].

Paschen's Curve is useful graphs that show breakdown voltages for a given pressure and separation product. Each gas has its own curve. Properly these should have the product on the x axis but it is usually more practical to assume normal atmospheric pressure and give separations on the x axis. Paschen's Law can be used to convert graphs with different axes [18].

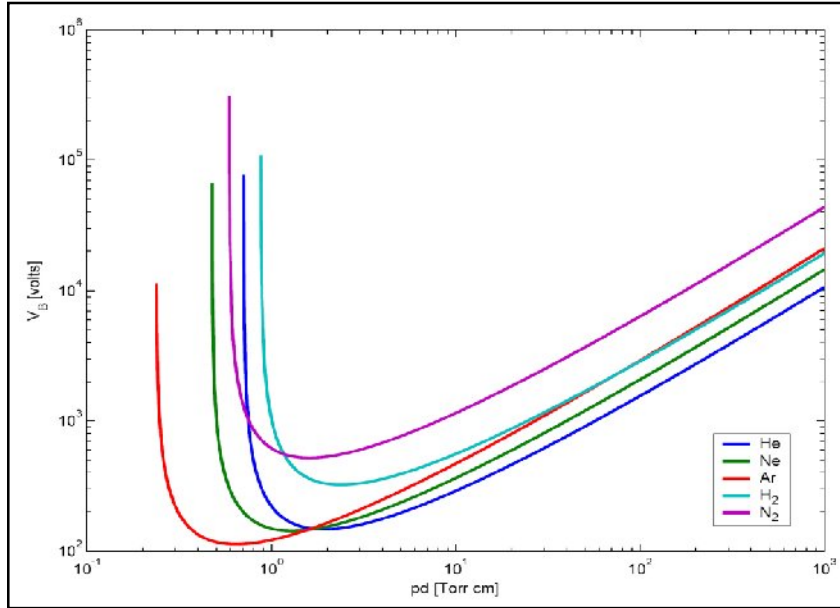


Figure 13: Paschen's Curve

Table 4 shows the minimum breakdown voltages for various gases are calculated using Equation 2.6 from Paschen's law.

Table 4: Minimum breakdown voltage for various gases

Gas	$V_{bd \text{ min}}$ (V)	$pd$ at $V_{bd \text{ min}}$ (torr cm)	Gas	$V_{bd \text{ min}}$ (V)	$pd$ at $V_{bd \text{ min}}$ (torr cm)
Air	327	0.567	N <sub>2</sub>	251	0.67
Ar	137	0.9	N <sub>2</sub> O	418	0.5
H <sub>2</sub>	273	1.15	O <sub>2</sub>	450	0.7
He	156	4.0	SO <sub>2</sub>	457	0.33
CO <sub>2</sub>	420	0.51	H <sub>2</sub> S	414	0.6

## 2.6 XPDC1 code

XPDC1 code is a bounded electrostatic code for simulating a 1-dimensional plasma discharge, running on UNIX workstations with X-Windows and PC's with an X-Windows emulator.

This code simulates a bounded cylindrical plasma discharge with the characteristics of which are specified by the user at run time using an input file. The discharge power comes from an axial source and can be specified as one of an axial electric field, discharge current or power.

The simulation can proceed in real-time, with the user viewing output as the codes run in the form of various user specified diagnostics which are updated each time step. The code compiles with standard C compiler and requires X-Windows libraries [19].

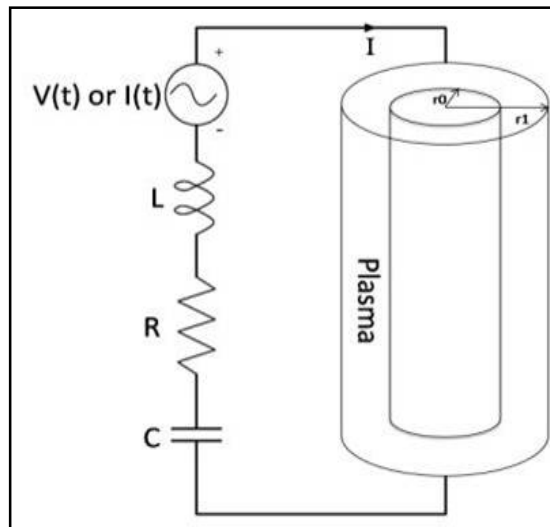


Figure 14: Cylindrical shape ionization gas sensor

## CHAPTER 3 METHODOLOGY

### 3.1 Procedure Identification

The work flow for this project is shown in the figure below.

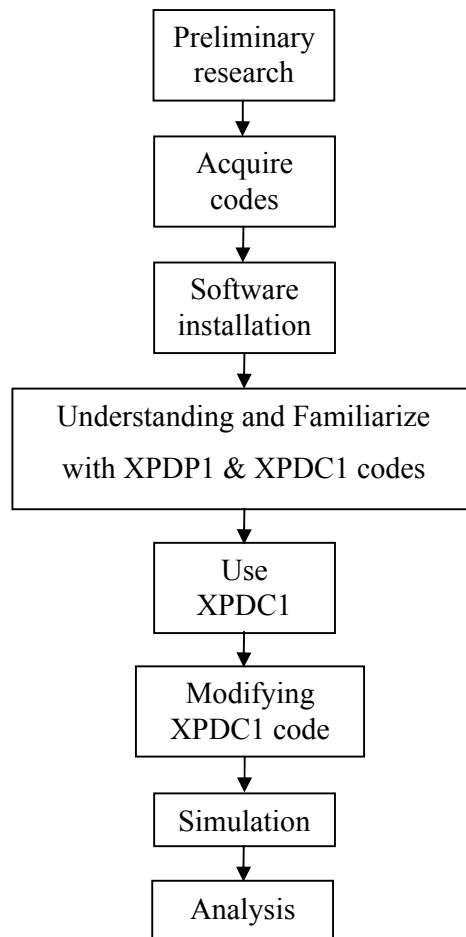


Figure 15: Work flow for completing the simulation

The work steps for completing this project are shown in Figure 10. It begins with preliminary research and study about the topic. Several journal and web page related to this project has been studied in order to understand the basic principles and operations of the gas sensor.

Then, the simulation codes which are XPDP1 and XPDC1 are acquired from trusted webpage. The code is properly compiled in the computer system. After the code is properly compiled, learning process is commenced. This step is necessary for this project in order to understand and become familiar with the code.

The simulation process is initialized by varying the existing code with appropriate simulation parameters in XPDC1input file. The parameters for the cylindrical ionization gas sensor. The parameters are established from the several journals with related to this project.

After the parameters are being set in the input file, simulation process will take place and the result obtained will be studied. Thorough analysis will be made to the result and will be discussed in the following chapter. The result and analysis obtained will determine the achievability of this project.

### **3.2 Tools and Equipments**

#### Softwares

1. XPDP1
  - Simulation code for parallel-pane plasma discharge.
  
2. XPDC1
  - Simulation code for cylindrical plasma discharge.
  
3. Origin Pro 8
  - Graph plotting software.



## **CHAPTER 4**

### **RESULT AND DISCUSSION**

#### **4.1 Result**

After the simulation, all the results are shown and will be discussed in this section. The result is important to be noted as it may give an explanation about the breakdown behaviours of the cylindrical shaped ionization gas sensor. In this section, the results would be explained generally based on the trends that can be observed. The results would be arranged according to the type of experiments done.

For investigating the behaviour of the sensor during breakdown, the radius of electrodes is made as the variable parameters. As the radius of the electrodes changes, the curvature of the electrodes also changed. Since a cylinder is round in one direction, one thinks of it as curved. It is its extrinsic curvature which it has in relation to the flat three-dimensional space it is part of. A cylinder can be made by rolling a flat piece of paper without tearing or crumpling it, so the intrinsic geometry is that of the original paper which is flat. This means that the distance between any two points is the same as it was in the original paper. Also parallel lines remain parallel when continued [13].

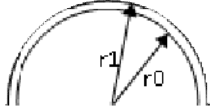
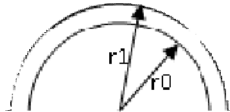
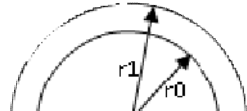
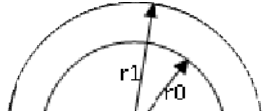
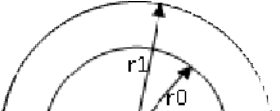
#### *4.1.1 Experiment 1: $r_0$ Fixed, $r_1$ Varied*

The first experiment is conducted to study the effect of varying the outer electrode radius. The initial setting for both inner and outer electrodes is determined based on the study conducted regarding the size of the sensor. The gas sensor currently in the market has been studied, and it gives the idea in determining the appropriate setting for the sensor.

The outer electrode radius in this experiment is set to be as small as possible to give the minimum distance between inner and outer electrode. Then, the radius is increased to as large as it can as long as it does not bigger than the commercial gas sensor. The illustration about this setting is shown in Table 5. Inner electrode radius is represented as  $r_0$  and  $r_1$  represent the outer electrode radius.

The important aspect that will be looking in this experiment is the sensor breakdown. This experiment will determine which value of electrodes setting can cause the sensor to breakdown and the behaviour of the sensor during breakdown will be discussed later in this section.

Table 5: Electrodes setting for Experiment 1

Electrodes setting	Electrodes illustrations
$r_0=0.01\text{m}$ $r_1=0.02\text{m}$	
$r_0=0.01\text{m}$ $r_1=0.04\text{m}$	
$r_0=0.01\text{m}$ $r_1=0.06\text{m}$	
$r_0=0.01\text{m}$ $r_1=0.08\text{m}$	
$r_0=0.01\text{m}$ $r_1=0.1\text{m}$	

The behaviour of the sensor is studied during the beginning of the simulation, after a period of time after the simulation begin, during breakdown and after a period of time after breakdown occurred.

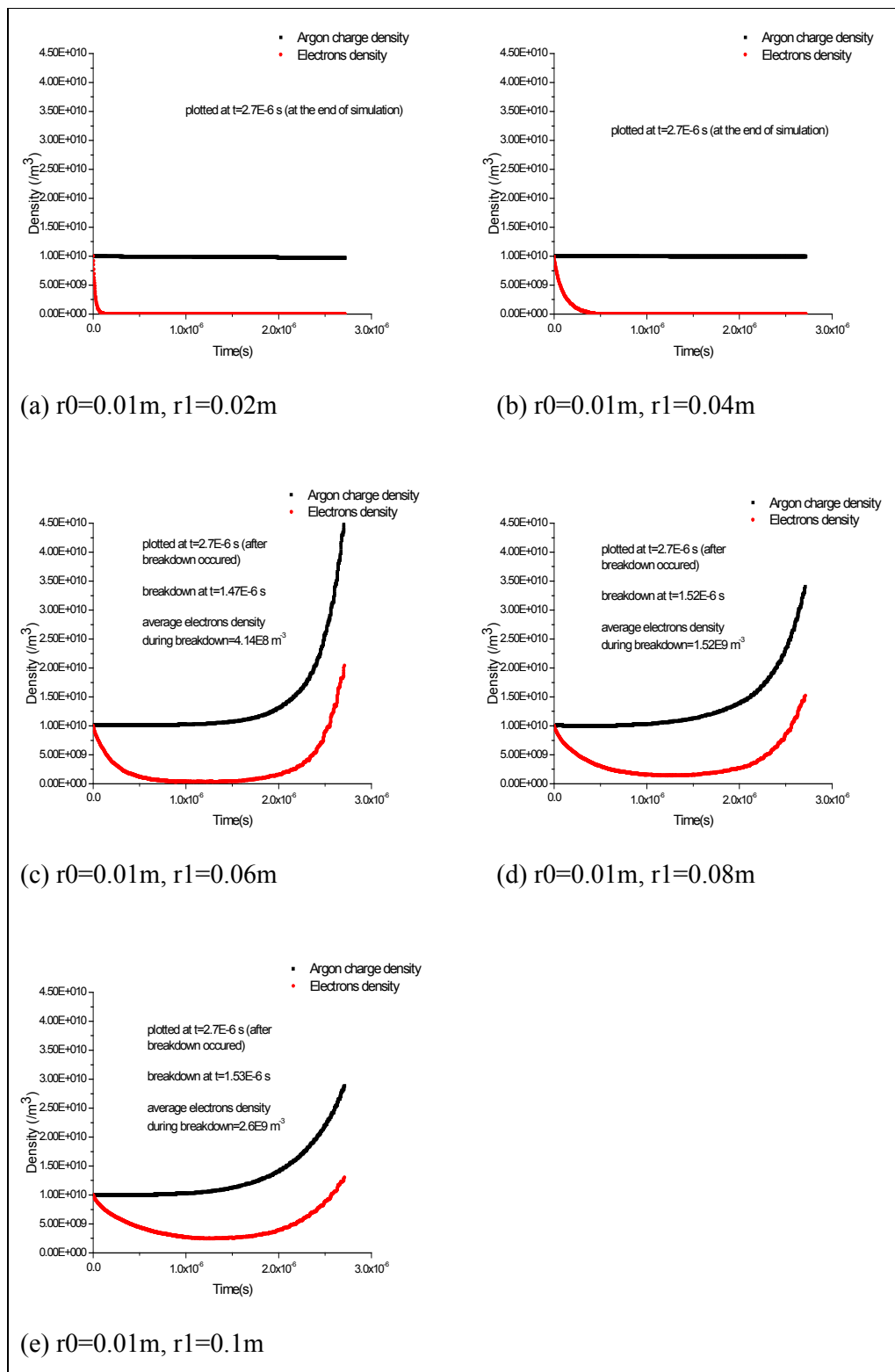


Figure 16: Average density versus time

Figure 16 shows the result obtained at the end of the simulations. The graphs in Figure 16 show average electrons density with respect to the time of the simulation. Noticed that, the end time for all simulations are the same. The simulation is stopped at  $t= 2.7E-6$  seconds. However, in real world, the time taken for each simulation is approximately 5 minutes. This is due to the step time parameter that being set in the input file.

For the first two simulations which used 0.02m and 0.04m for r1, the graph plotted is different from when r1 is set to 0.06m, 0.08m and 0.1m respectively. The average electrons density is decreased to zero throughout the simulation. This is because the effect of the sheath formation between electrodes. However, all simulations showed that the density of electrons reduced initially for all electrodes setting.

Larger r1 setting resulted different graphs. Average electrons density observed to be increased after a period of time. It keeps increasing until the simulation stopped. This is due to the ionization processes which produced electrons and resulted to the sensor breakdown. This topic will be discussed later in this section.

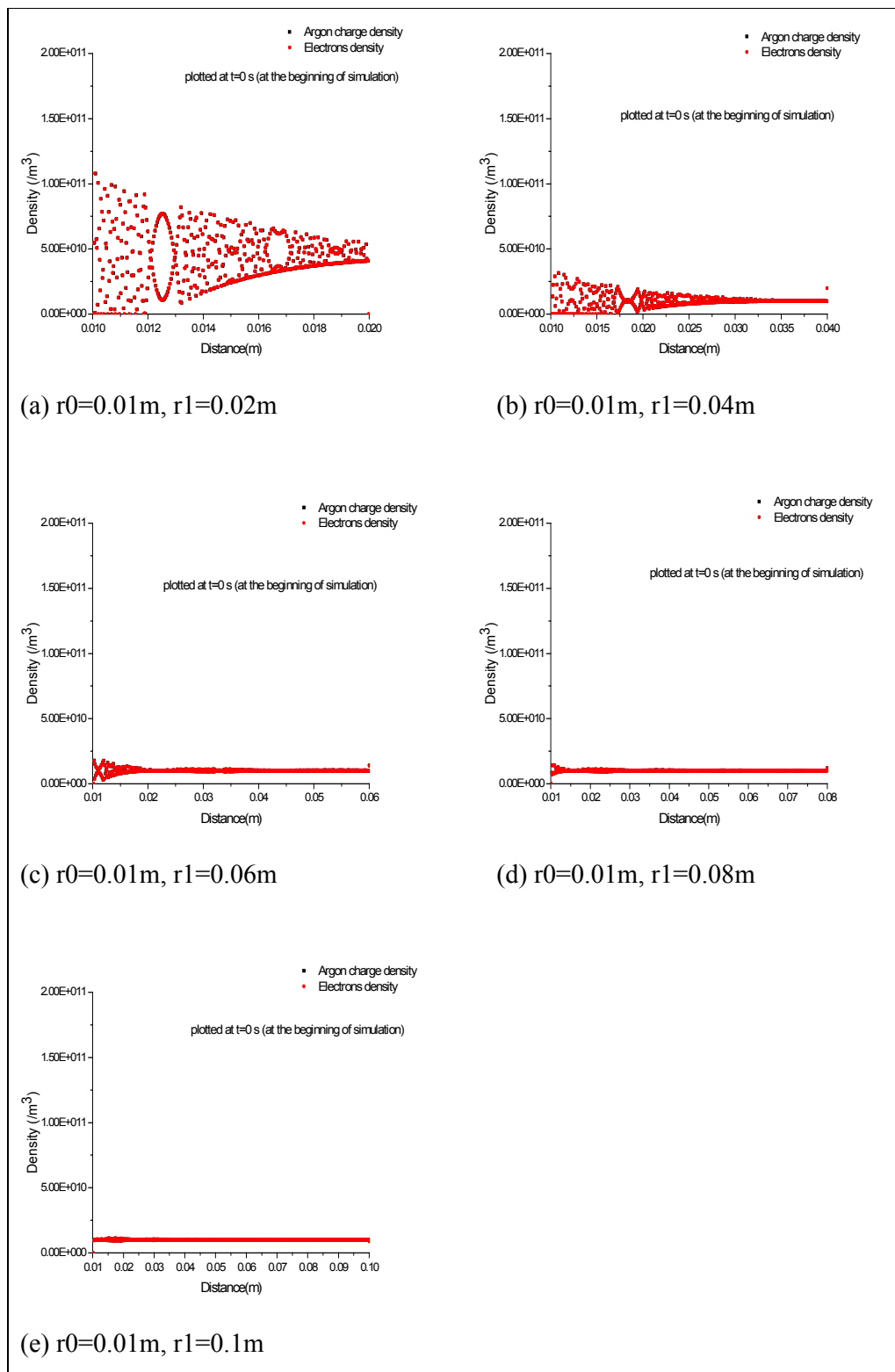


Figure 17: Density versus electrodes spacing at  $t=0$  s

Figure 17 shows the result obtained at  $t=0$  which is the beginning of the simulation. The graph plotted shows electrons and Argon charges density between electrodes. Figure 17(a) clearly shows that electrons and Argon charges are higher towards inner electrode. Due to smaller radius of outer electrode, the gap between electrodes is small, thus, the volume is smaller and the space to be occupied by electrons and Argon charges is small. This will make electrons and Argon charges to be packed in the region. Figure 18 shows the arrangement for anode and cathode for this experiment.

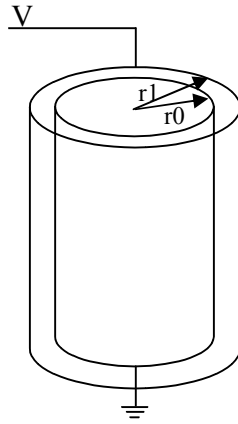


Figure 18: Arrangement for cathode and anode

Since inner electrode is the cathode, electrons are observed to be higher close to its surface. This effect is shown in Figure 19. It shows the comparison for electrons and Argon charges density for different electrodes setting. The red dots represent electrons while black dots represent Argon charges in the gas sensor.

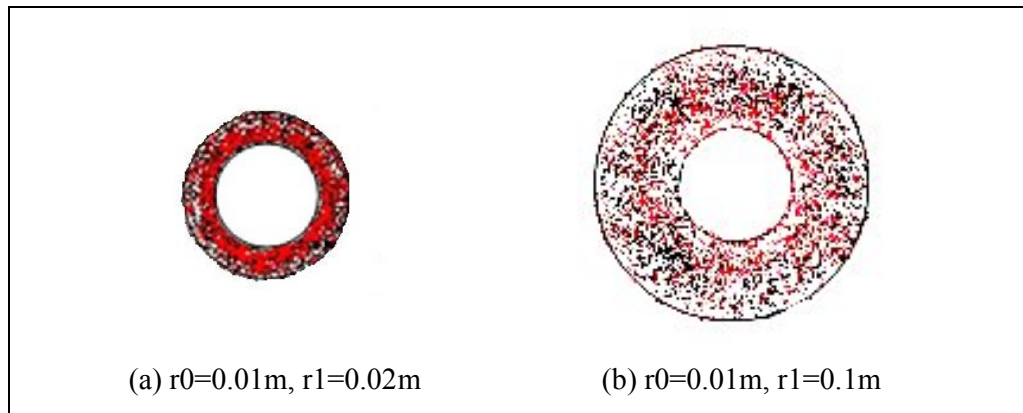


Figure 19: Electrons and Argon charges between electrodes

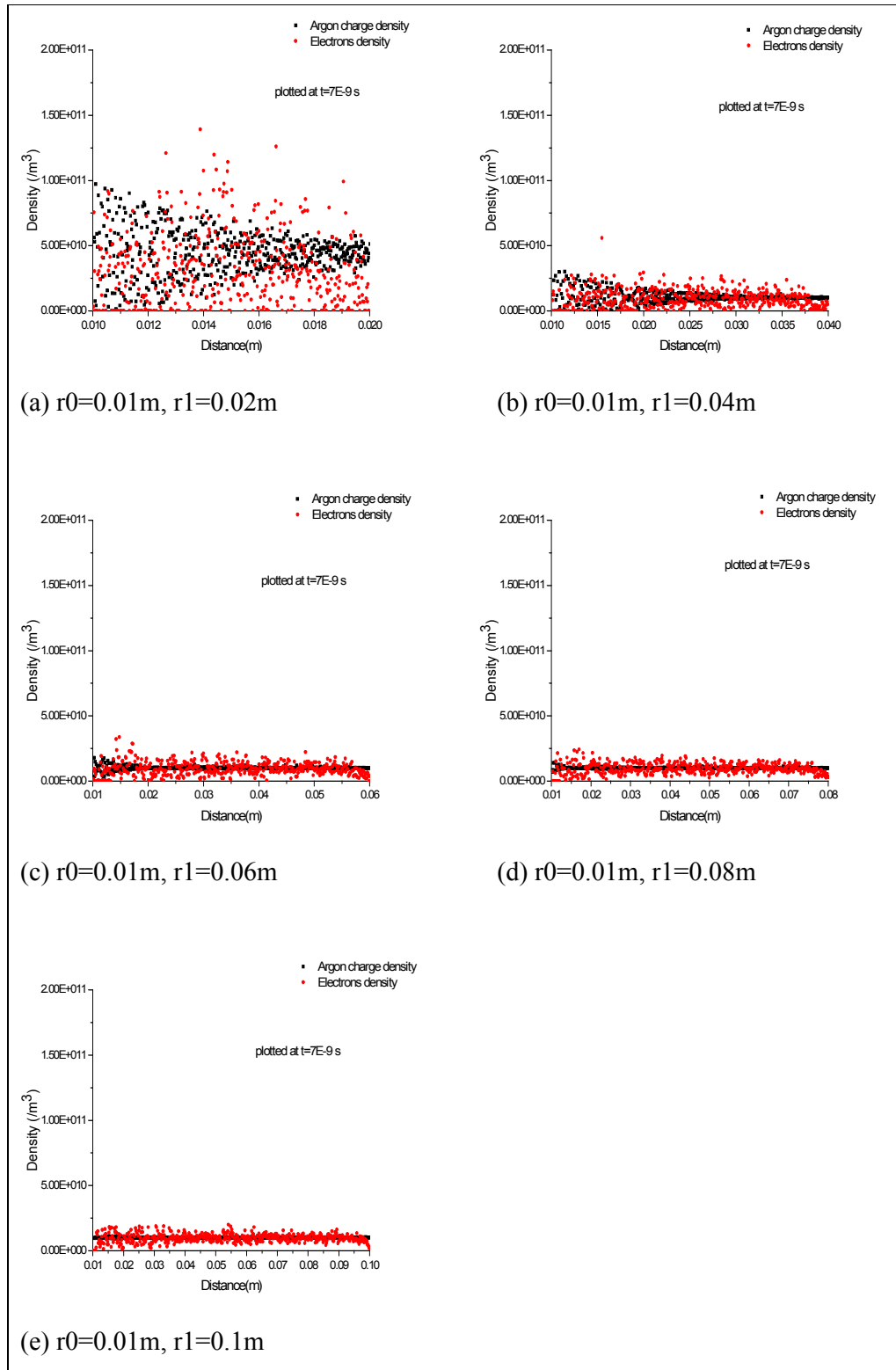


Figure 20: Density versus electrodes spacing at  $t=7E-9$  s



Figure 20 shows the result obtained after a certain period after the simulation begin. It is plotted at  $t=7E-9$  seconds. From the graphs in Figure 20, notice that the density of electrons is observed to be arbitrary. The bias applied to the sensor has caused this effect. When the bias applied to anode, electric field is formed between both electrodes and causes electrons gained energy. The energy gained will increase the mobility of electrons and lead to the recombination and reproduction of electrons.

However, this effect is less significant when the simulation is running with larger value of  $r$ . For instance, the simulation for 0.06m 0.08m and 0.1m of  $r_1$  resulted in better plot and can be seen in Figure 20(c), (d) and (e) respectively. Larger outer electrode radius means the distance between electrodes is larger, thus, this will reduce the effect of electrons recombination and reproduction due to the bias applied to the sensor.

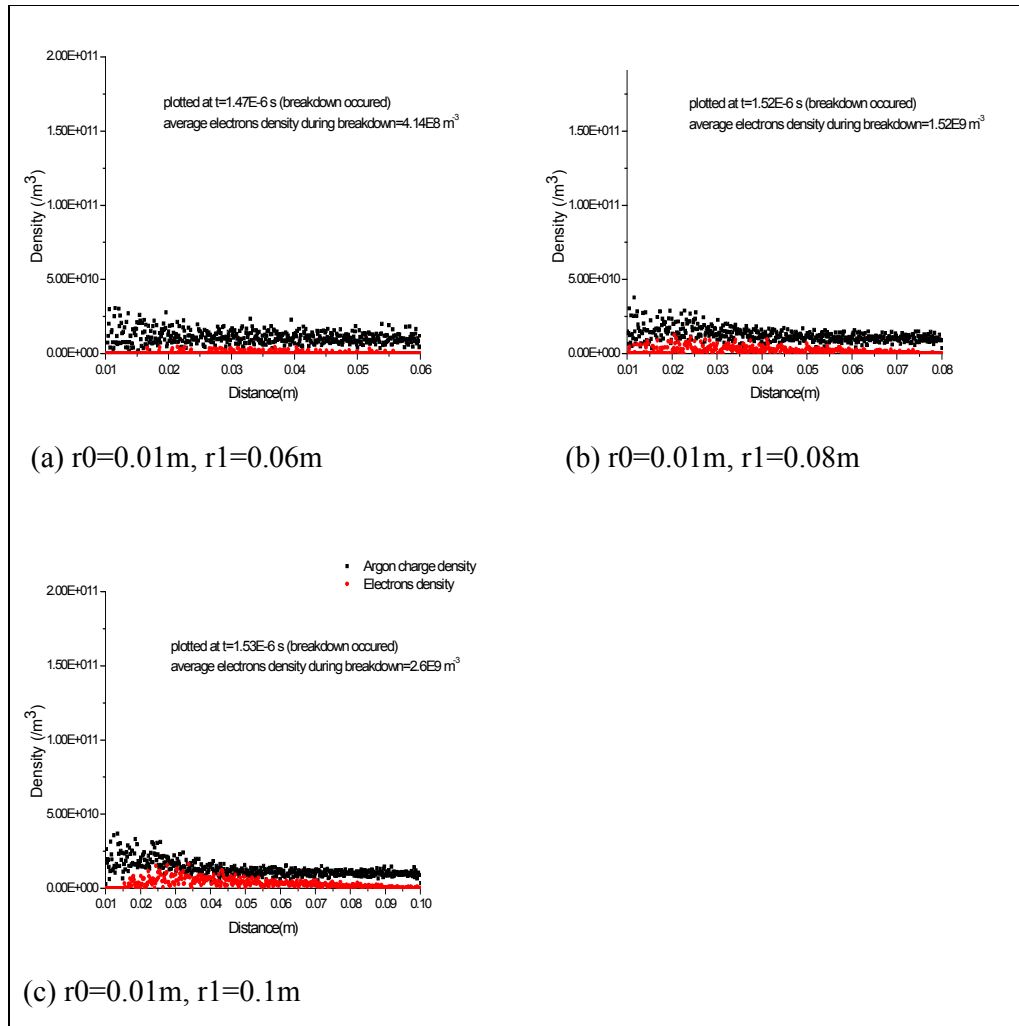


Figure 21: Density versus electrodes spacing at breakdown

Figure 21 shows the result for the simulation when the sensor is breakdown. Noticed that, for  $r_1=0.02\text{m}$  and  $r_1=0.04\text{m}$ , there is no plot for both simulation in Figure 21. It is due to the fact that both simulations did not cause the sensor to undergo breakdown phase.

The fact that sheath formed between electrodes has caused the sensor to not breakdown when  $r_1$  is set to  $0.02\text{m}$  and  $0.04\text{m}$ . This effect will be further discussed afterward.

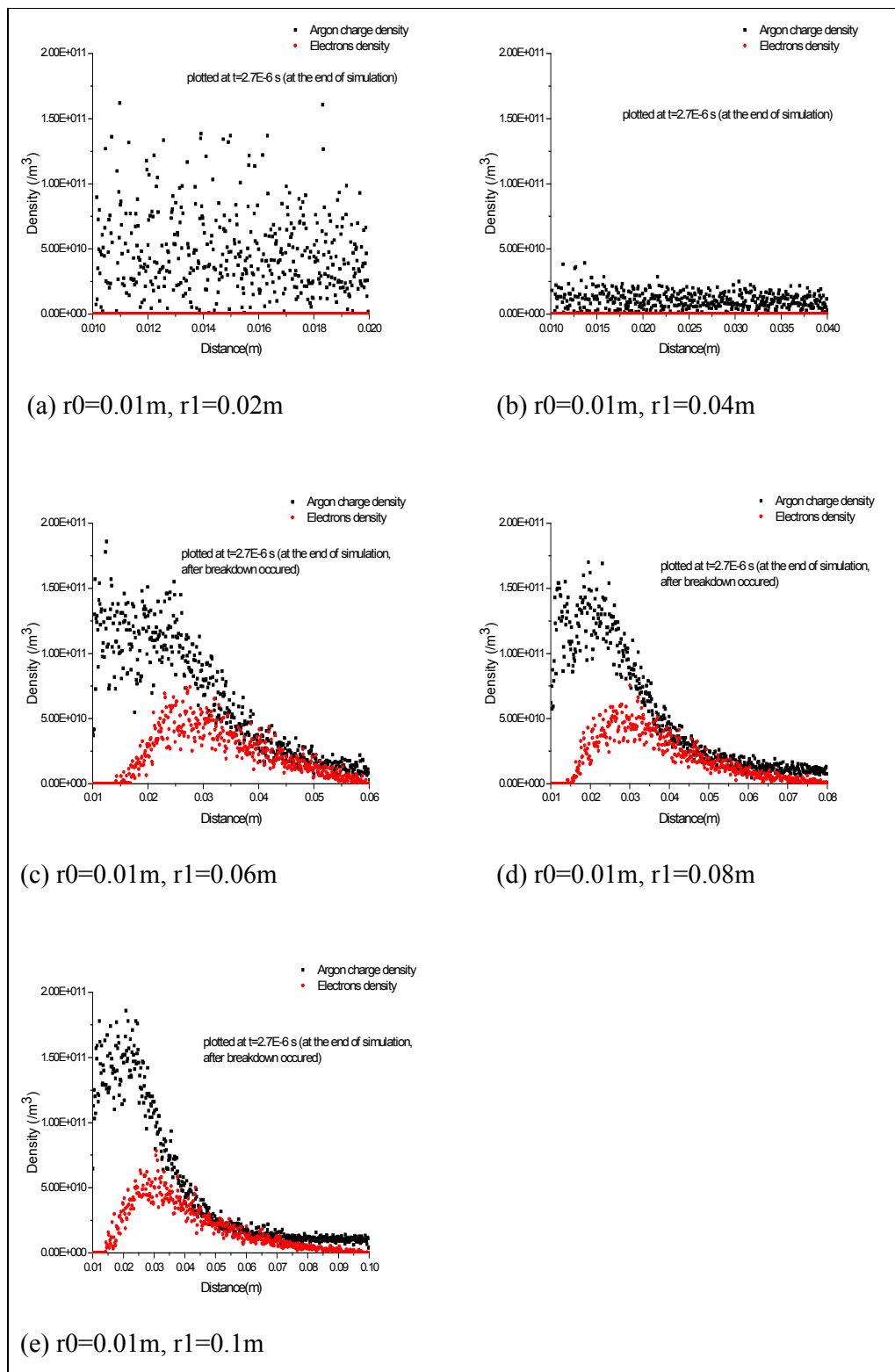


Figure 22: Density versus electrodes spacing at  $t = 2.7 \times 10^{-6}$  s

Figure 22 shows the result for electrons and Argon charges density between electrodes at the end of simulation for each electrodes setting. When breakdown has occurred, the sensor stated to conduct electricity and current can passed the dielectric medium freely. This is due to the fact that number of electrons between two electrodes has been increased due to the ionization processes that happen.

The pattern for the plot is observed to be the same when simulation is running with  $r_1$  set to 0.06m, 0.08m and 0.1m. The sheath effect can be clearly seen in this graph where the number of electrons is significantly small at the border of both electrodes.

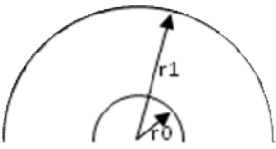
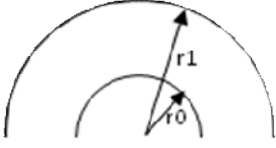
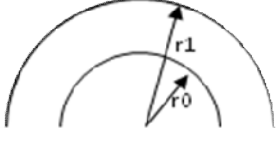
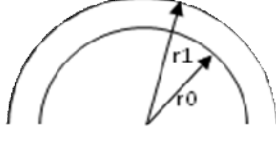

#### 4.1.2 *Experiment 2: $r_0$ Varied, $r_1$ Fixed*

The experiment is continued with a different method. Previously, Experiment 1 is conducted to check the curvature effect of outer electrode to the breakdown behaviour of a cylindrical-shape gas sensor. Then, the next experiment will vary the inner electrode radius and keeping the outer electrode at its maximum radius.

In this experiment, the effect of varying the curvature of inner electrode will be investigated. The value set for inner electrode is complied with the standard value for the commercial gas sensor. The value is set from as small as possible to its maximum as possible. In other word, the inner electrode is set from distant to be closer to the outer electrode. The electrodes setting are illustrated in Table 6.

The analysis done in Experiment 2 is the same analysis for Experiment 1 where the result is analyzed at the beginning, after a period of time after the simulation begin, during breakdown and after a period of time after breakdown occurred. Basically, Experiment 2 is a repetition of Experiment 1 but using  $r_0$  as the variable parameter.

Table 6: Electrodes setting for Experiment 2

Electrodes setting	Electrodes illustrations
$r_0=0.01\text{m}$ $r_1=0.1\text{m}$	
$r_0=0.03\text{m}$ $r_1=0.1\text{m}$	
$r_0=0.05\text{m}$ $r_1=0.1\text{m}$	
$r_0=0.07\text{m}$ $r_1=0.1\text{m}$	
$r_0=0.09\text{m}$ $r_1=0.1\text{m}$	

The result obtained from this experiment will determine the value of  $r_0$  that can cause the sensor to breakdown. Notice that, the distance between inner and outer electrodes for this experiment is the same as the distance between electrodes for Experiment 1. Distance between electrodes also known as electrodes spacing is simply calculated by subtracting  $r_1$  with  $r_0$ .

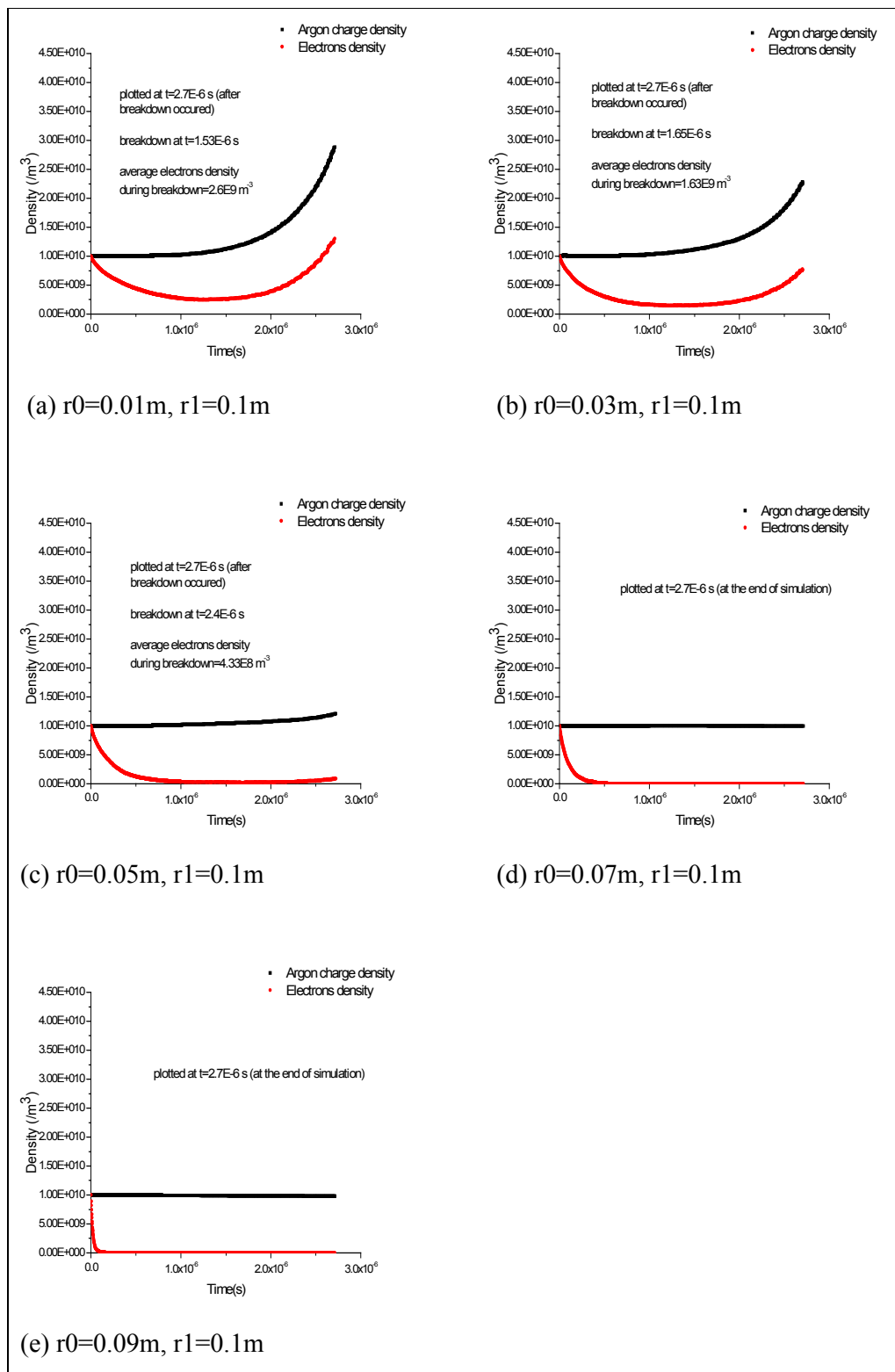


Figure 23: Average density versus time

Figure 23 is the result obtained from the simulation with various values of  $r_0$ . Figure 23 shows average density for electrons and Argon charges with respect to simulation time. The graphs plotted in Figure 23 are similar to the graphs plotted in Figure 16. Their pattern is the same. Electrons and Argon charges density are observed to follow the pattern whereby it experiencing the electrons reduction before it increases for a certain electrodes spacing.

When the electrodes are set to be 0.05m or 0.07m or 0.09m away from each other, the graph in Figure 23 (a), (b) and (c) will be obtained. However, if the electrodes spacing is 0.01m or 0.03m away from each other, it will give Figure 23(d) and (e) whereby the electrons density is zero throughout the simulation. From the plot from Figure 16 and Figure 23, an early conclusion can be made such that the sensor undergo breakdown only if the electrodes spacing is greater than 0.03m.



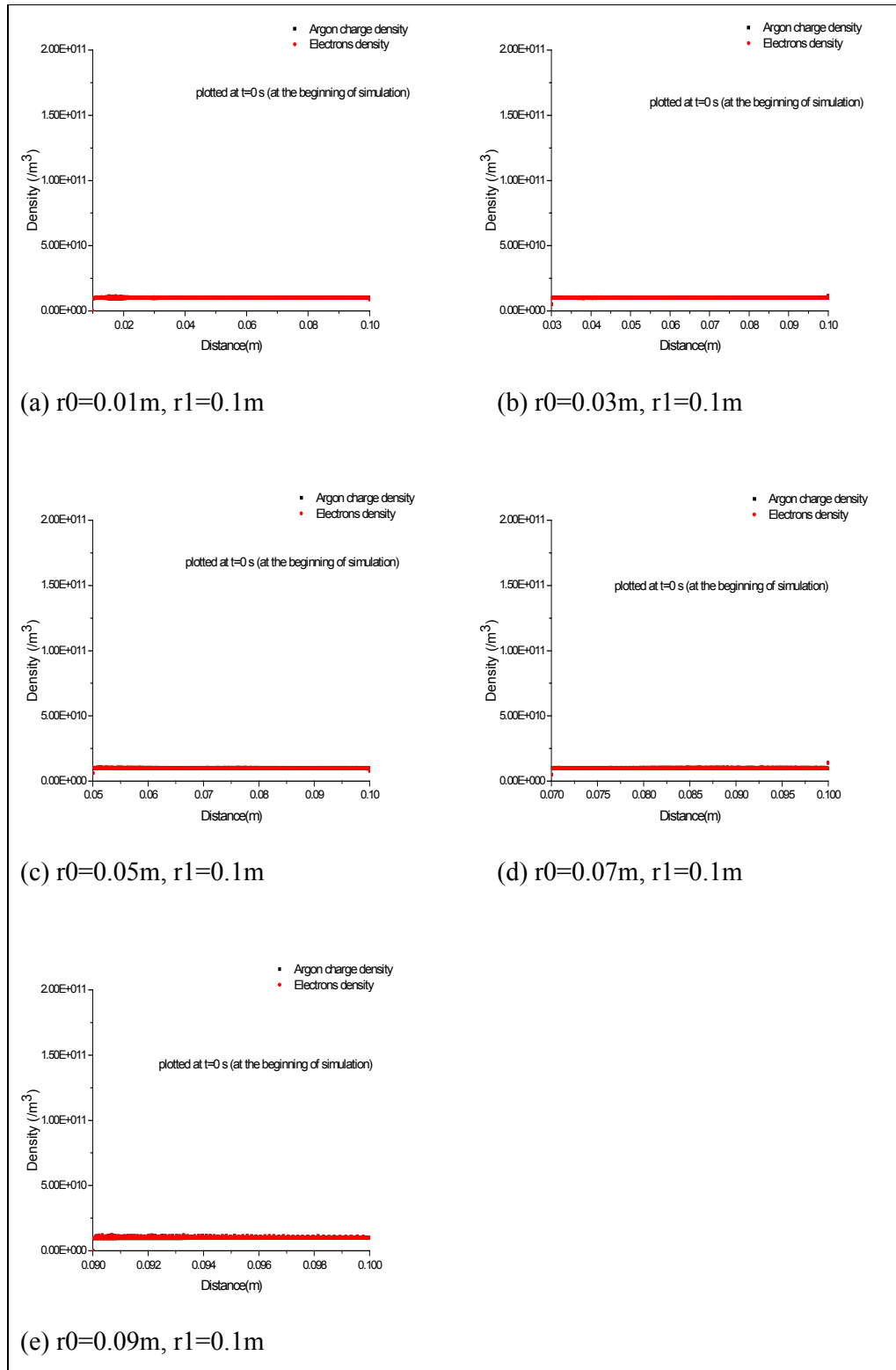


Figure 24: Density versus electrodes spacing at t=0 s

Figure 24 shows the density of electrons and Argon charges at the beginning of the simulation. As an extension from Experiment 1, noticed that the plot is different from Figure 17 whereby the density for electrons and Argon charges is uniformly distributed between electrodes and the number is equal to the input value for electrons and Argon charges. It is not as packed as in Experiment 1 even though the spacing for electrodes is set to be the same for both experiments.

As the inner electrode is configured to be cathode in this simulation, the surface of the cathode will influence the distribution of the charges. As  $r_0$  is increased and  $r_1$  is fixed at 0.1m, the inner electrode is expand and became closer to the outer electrode, the volume for electrons and Argon charges to occupy the space between electrodes will be smaller and the space will be packed with electrons and Argon charges. However, the surface area of inner electrode is increased as the electrode is getting bigger and caused electrons and Argon charges to be distributed evenly between electrodes. The effect can be clearly seen in Figure 24.

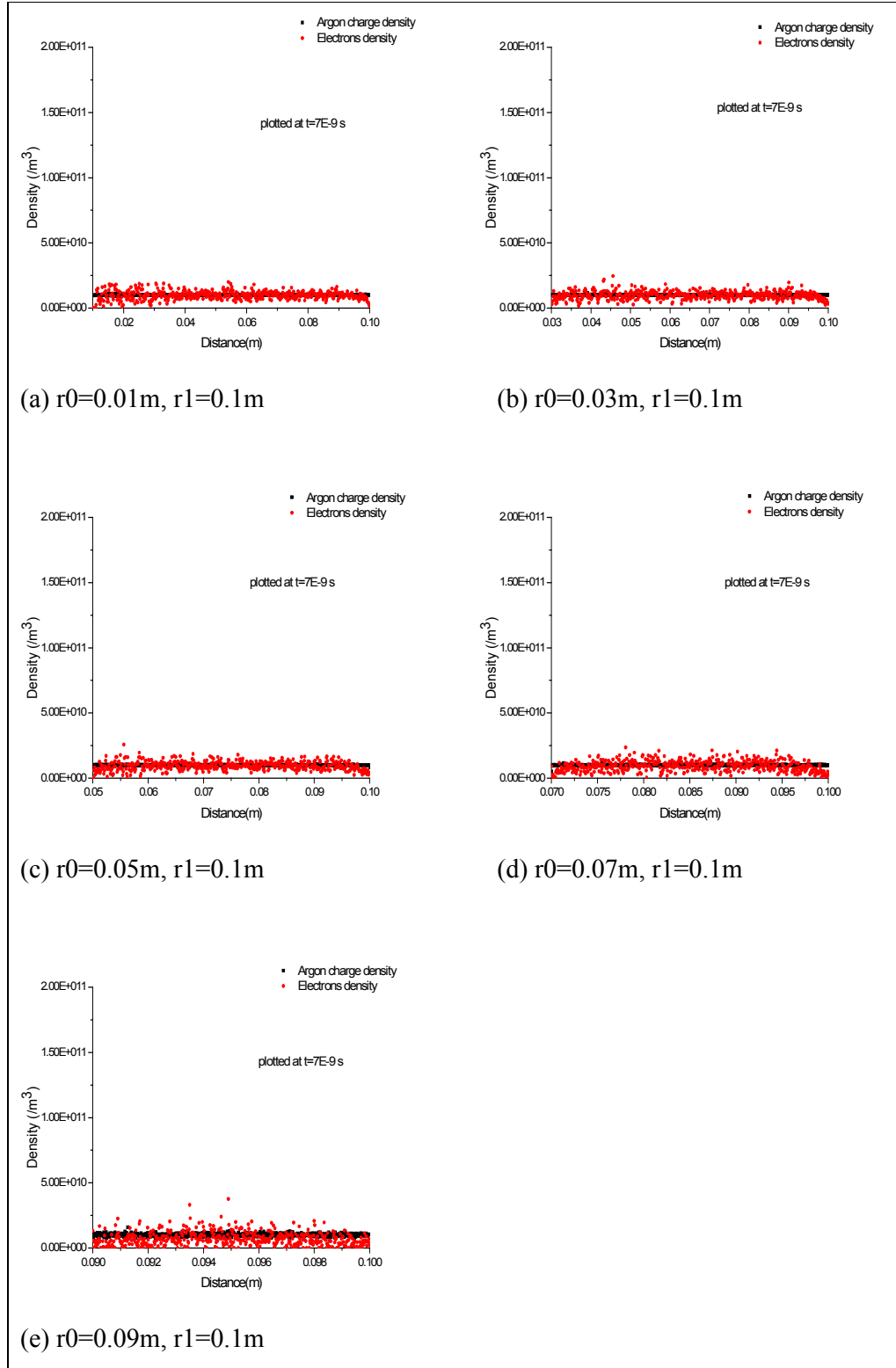


Figure 25: Density versus electrodes spacing at  $t=7E-9$  s

When voltage source is applied to the sensor, the result of the biasing is shown in Figure 25 where it can be noticed that the graph pattern is the same as in Figure 20. The number of electrons is arbitrary along the electrodes spacing. Due to the electric field generated from the biasing, electrons gaining energy to drift along the electric field and collide with Argon atom and resulted in recombination and ionization. Thus, this will lead to the uncertainty of electrons density along the spacing.

The numbers of electrons appeared to be lower at the border of both electrodes. This is due to the sheath formation at the border of electrodes and caused electrons to be lower at the border. This effect will be discussed further in this section later.

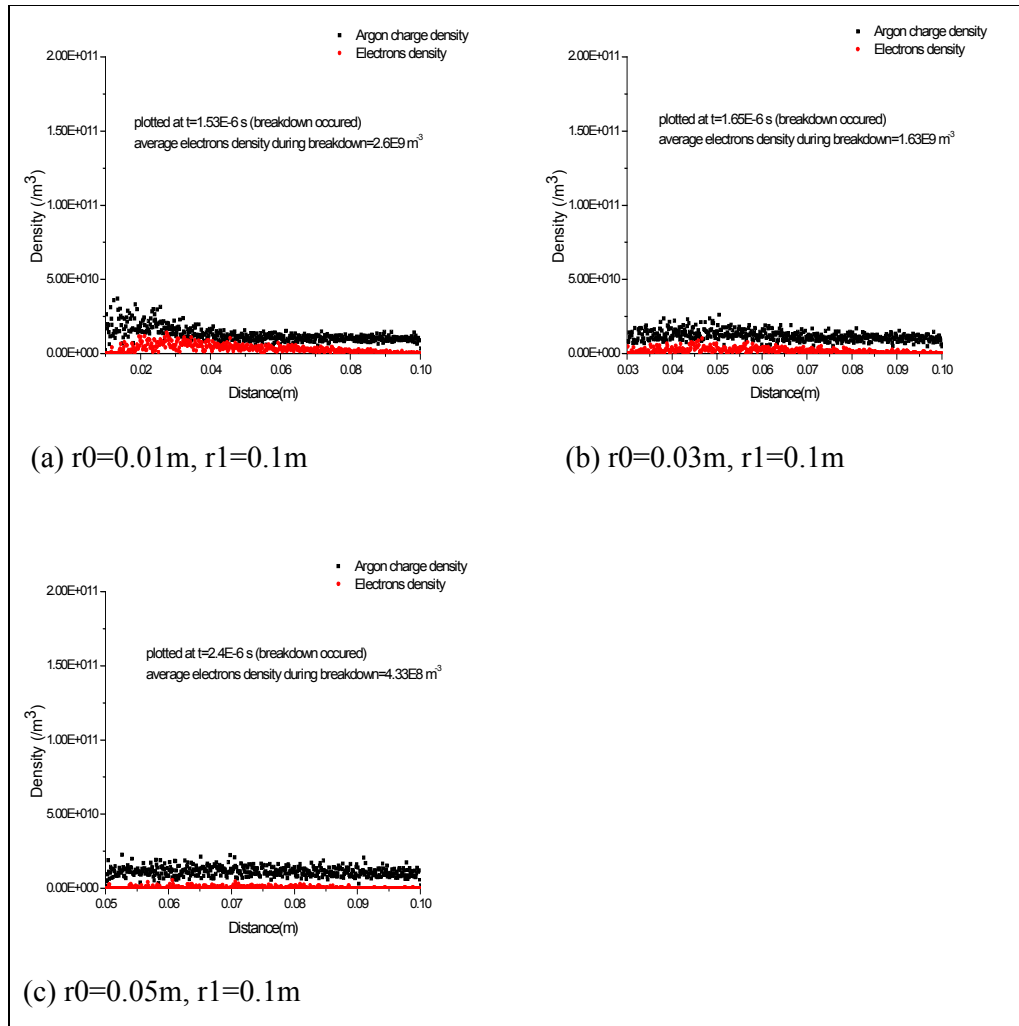


Figure 26: Density versus electrodes spacing during breakdown

Figure 26 shows the breakdown behaviour of the sensor. Since breakdown only occurred if the distance between electrodes is greater than 0.03m, the result obtained is for 0.05m, 0.07m and 0.09m of electrodes spacing. The graphs plotted clearly shows the effect of sheath formed to electrons density between electrodes.

The number of electrons is increased as the number of Argon charges increased because of the ionization by electron impact that produced free electrons and Argon charges. The time taken to produce enough electrons for the sensor to breakdown is the main interest for this experiment in order to improve its sensitivity.

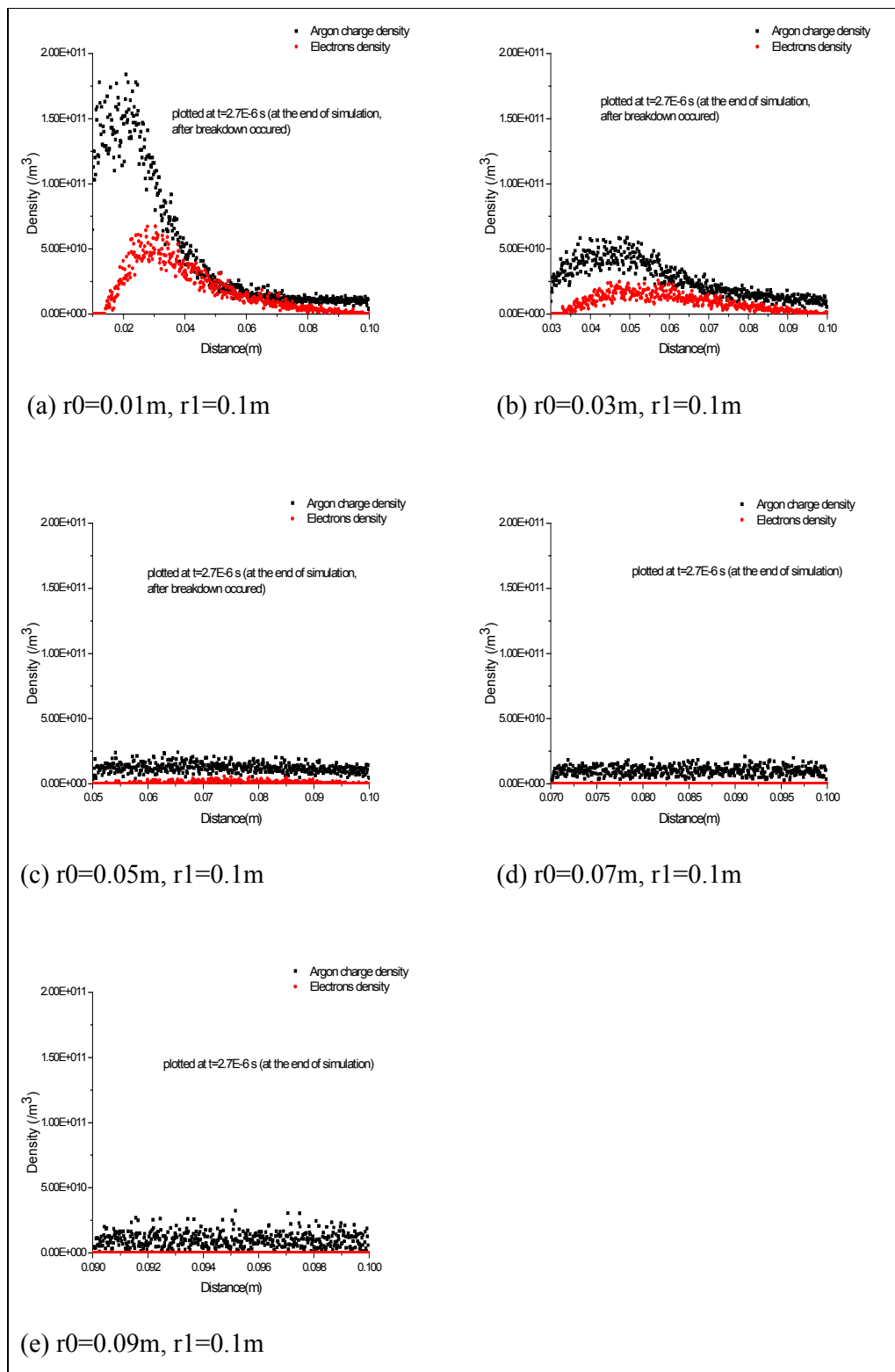


Figure 27: Density versus electrodes spacing at  $t = 2.7 \times 10^{-6}$  s

The simulation continues until  $t=2.7E-6$  s, the result obtained is shown in Figure 27. The result shows that the density of electrons and Argon charges is higher towards the inner electrode. However, for Figure 27(d) and (e), the number of electrons is zero at the end of simulation. This is due to several recombination factor that result in electrons quenching from the sensor. Not to forget, the effect sheath formed that only reside for positive Argon charges and caused the number of electrons to be reduces at the border of both electrodes.

The result from Experiment 1 and Experiment 2 has lead to the continuation of Experiment 3 whereby the simulation done with pressure variation. The electrodes setting for this experiment is determined from the previous experiments. Both methods used for the experiments respectively can cause the sensor to breakdown. Thus, Experiment 3 is conducted to determine which electrodes setting will cause the sensor to breakdown faster. This criteria is will make the sensor to be more sensitive

The pressure applied for previous two experiments is 1 torr. For experiment 3, the pressure is set to 10 torr, 100 torr and 1000 torr where the breakdown behaviour of the sensor is observed in term of the response time and also the electrons density observed during the sensor breakdown.

### 4.1.3 Experiment 3: Pressure Variation

#### 4.1.3.1 Experiment 3.1: $r_0=0.01m$ , $r_1=0.06m$ , pressure varied

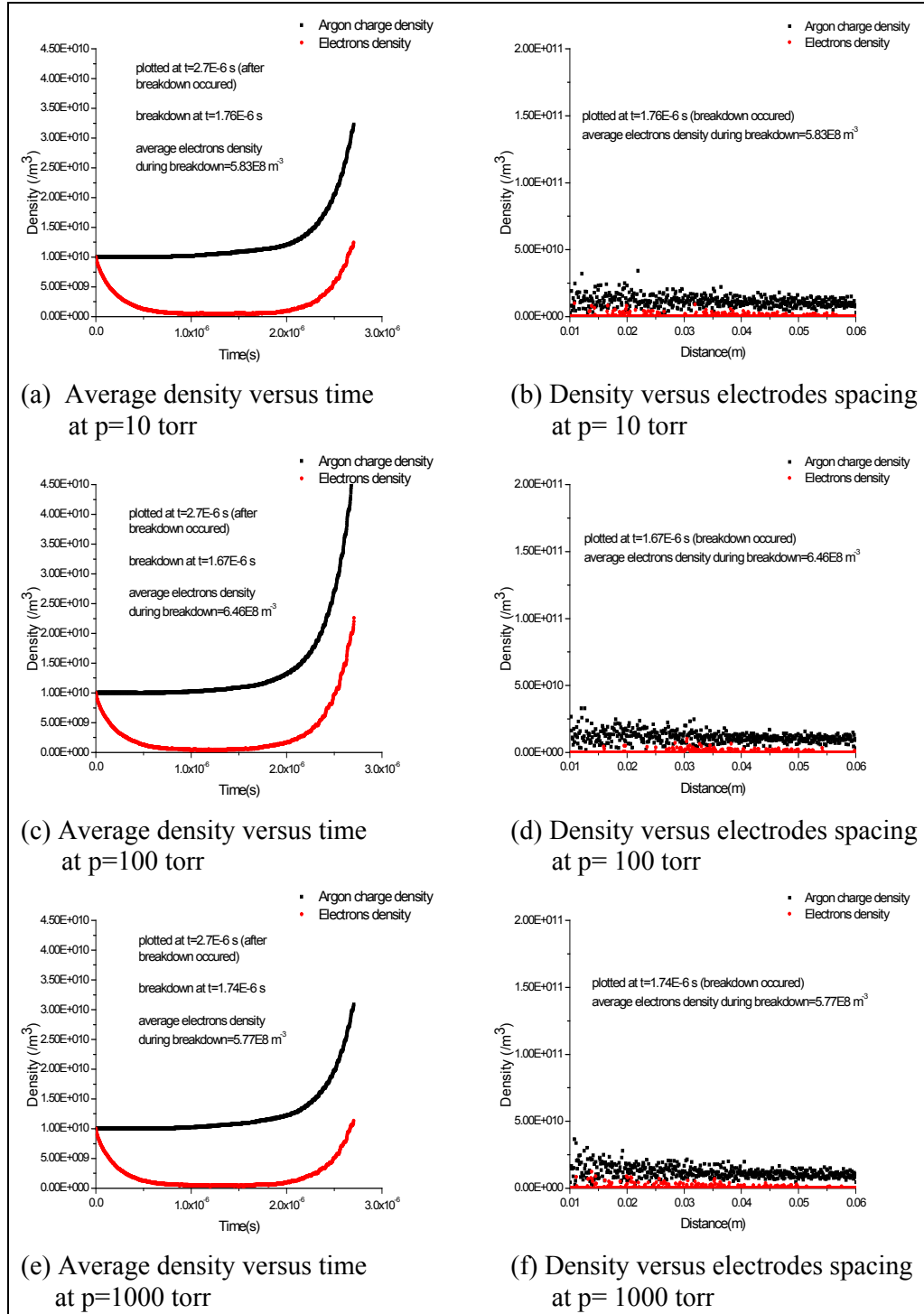


Figure 28 : Result obtained during breakdown for  $r_0=0.01m$  and  $r_1=0.06m$



4.1.3.2 Experiment 3.2:  $r_0=0.01m$ ,  $r_1=0.08m$ , pressure varied

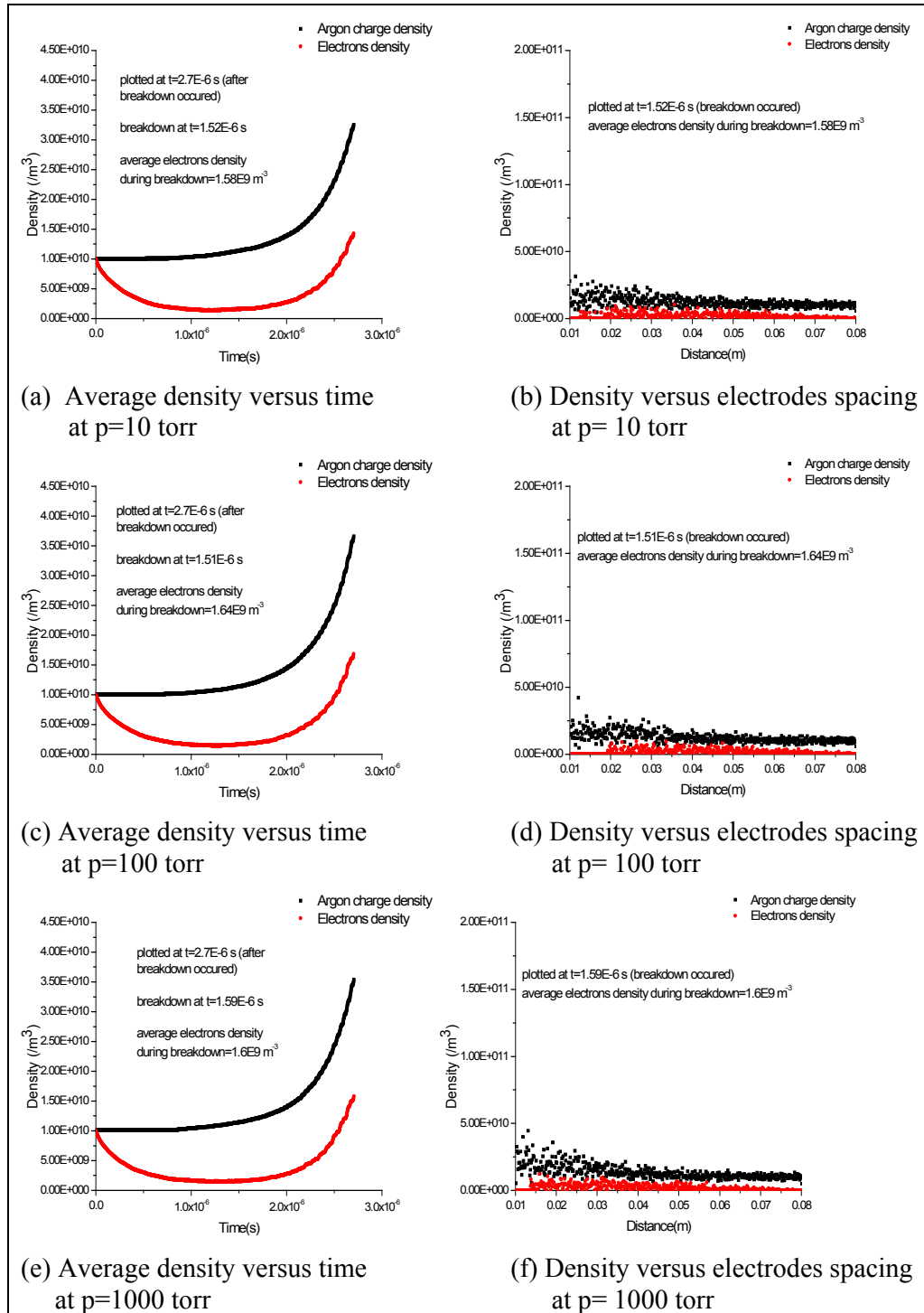


Figure 29 : Result obtained during breakdown for  $r_0=0.01m$  and  $r_1=0.08m$

4.1.3.3 Experiment 3.3:  $r_0=0.01m$ ,  $r_1=0.1m$ , pressure varied

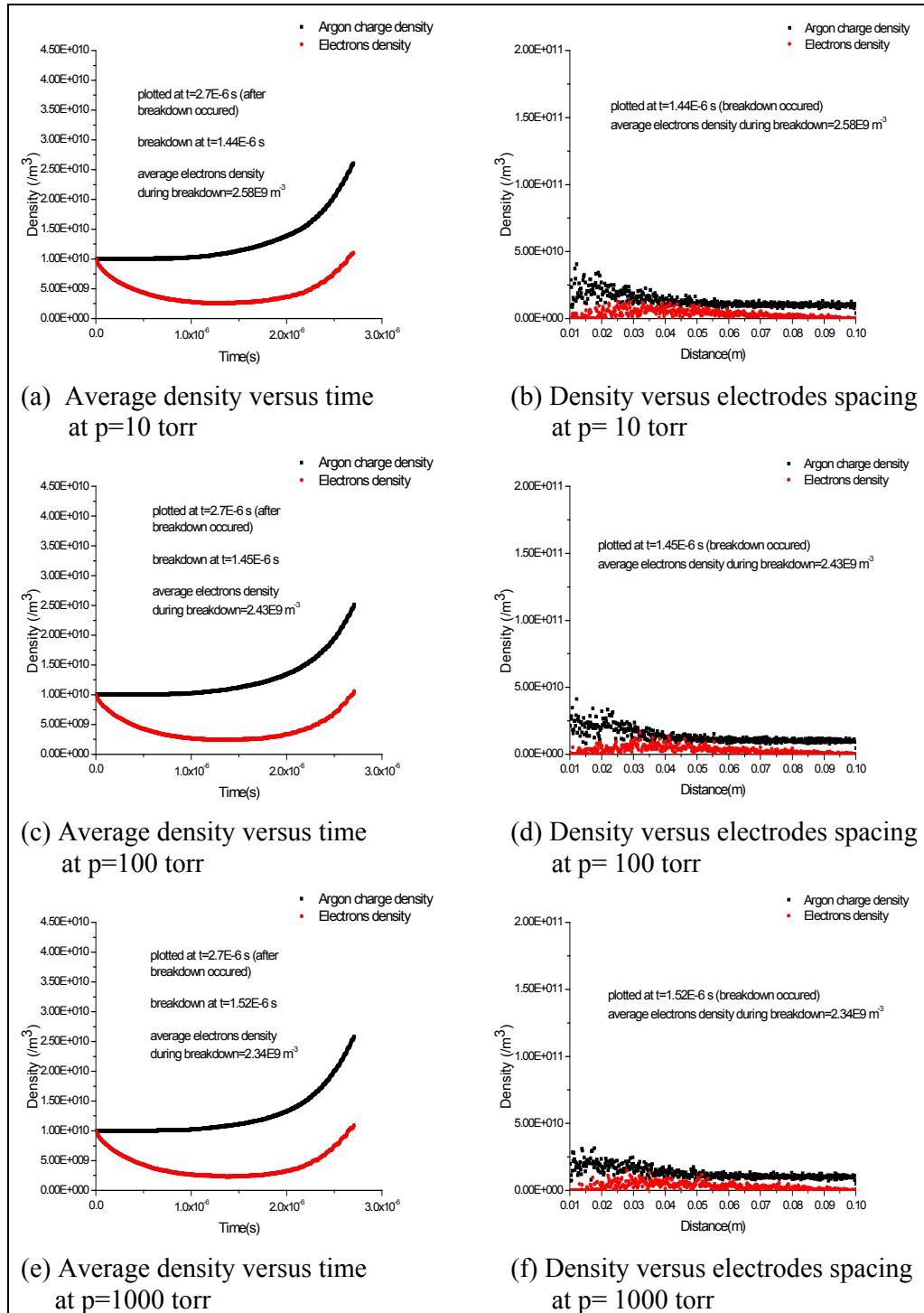


Figure 30: Result obtained during breakdown for  $r_0=0.01m$  and  $r_1=0.1m$

4.1.3.4 Experiment 3.4:  $r_0=0.03m$ ,  $r_1=0.1m$ , pressure varied

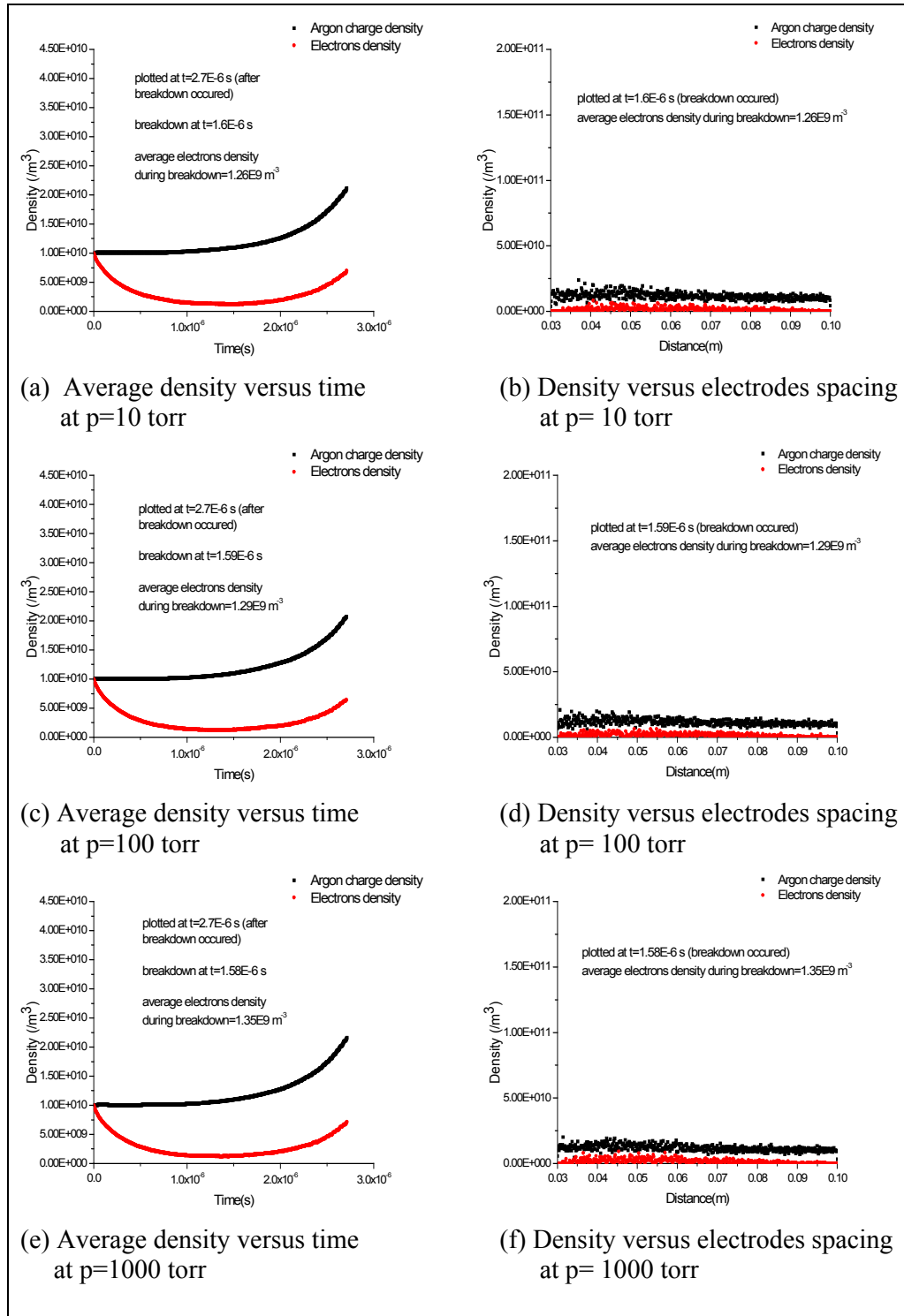


Figure 31: Result obtained during breakdown for  $r_0=0.03m$  and  $r_1=0.1m$

4.1.3.5 Experiment 3.5:  $r_0=0.05m$ ,  $r_1=0.1m$ , pressure varied

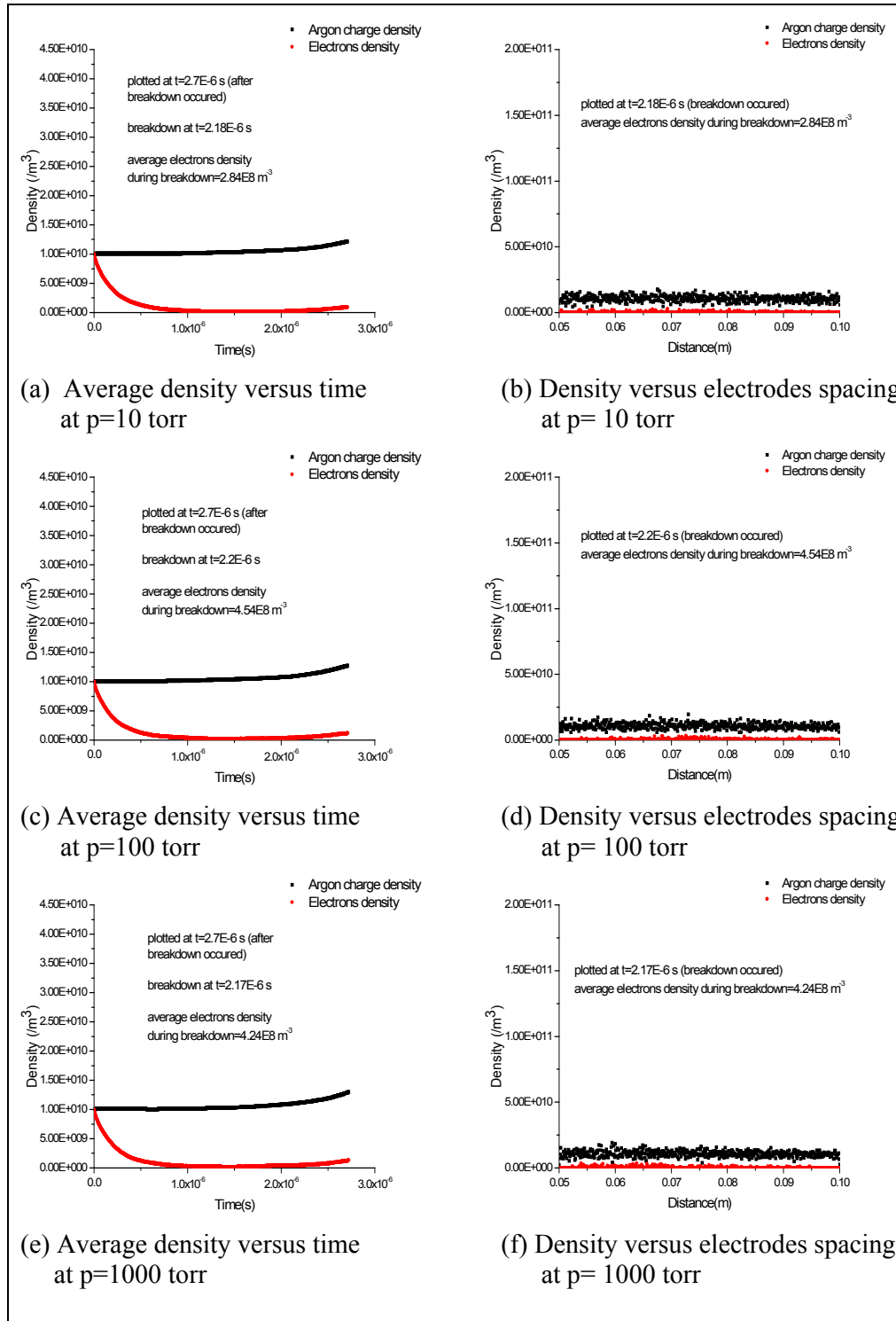


Figure 32 : Result obtained during breakdown for  $r_0=0.05m$  and  $r_1=0.1m$

After the simulation done, the result obtained for Experiment 3 is compiled and arranged in Table 7 and table 8 for more convenience view.

Table 7: Time taken for sensor to breakdown

	Outer electrode variation (r0 fixed at 0.01m, r1 varied)			Inner electrode variation (r0 varied, r1 fixed at 0.1m)		
Electrodes spacing, d, (m)	Time to breakdown (s)			Time to breakdown (s)		
	P=10 torr	P=100 torr	P=1000 torr	P=10 torr	P=100 torr	P=1000 torr
0.05	1.76E-6	1.67 E-6	1.74 E-6	2.18 E-6	2.2 E-6	2.17 E-6
0.07	1.52 E-6	1.51 E-6	1.59 E-6	1.6 E-6	1.59 E-6	1.58 E-6
0.09	1.44 E-6	1.45 E-6	1.52 E-6	1.44 E-6	1.45 E-6	1.52 E-6

Table 8: Electrons density observed during breakdown

	Outer electrode variation (r1 varied)			Inner electrode variation (r0 varied)		
Electrodes spacing, d, (m)	Electrons density (m <sup>-3</sup> )			Electrons density (m <sup>-3</sup> )		
	P=10 torr	P=100 torr	P=1000 torr	P=10 torr	P=100 torr	P=1000 torr
0.05	5.83E8	6.46E8	5.77E8	2.84E8	4.54E8	4.24E8
0.07	1.58E9	1.64E9	1.6E9	1.26E9	1.29E9	1.35E9
0.09	2.58E9	2.43E9	2.34E9	2.58E9	2.43E9	2.34E9

The result showed that the pressure variations do not have significant effect to the time taken for the sensor to breakdown. However, the electrons density observed during the sensor breakdown is affected by pressure.

## 4.2 Discussion

The result obtained from the experiment is gathered and analyzed based on several criteria for further understanding about the behaviour of the sensor.

The initial electrons and Argon charged density are set to be  $1E10 \text{ m}^{-3}$  for the all experiments. The density set to this value because the experiment is to study on the low density Argon discharge in cylindrical shape gas sensor. In industrial application, ionization gas sensor is deployed at a confined area where lot of gases presence and can flow into the chamber then react with the sensor to cause breakdown.

### 4.2.1 *Electrons loss mechanisms*

Average density versus time graphs plotted for each experiment showed that for every simulation, the density for electrons and Argon charges are decreased initially before they increased after certain period. However, some of the graphs plotted did not show any increases in electrons density when the electrodes spacing being set for the simulation,  $d=0.01\text{m}$  and  $0.03\text{m}$ . Noticed that, for Experiment 1, electrons density is decreased until zero but Argon charges remained at  $1E10 \text{ m}^{-3}$  until the simulation ended at  $t=2.7E-6 \text{ s}$  for  $r1=0.02\text{m}$  and  $r1=0.04\text{m}$ . When  $r1$  is set for  $0.06\text{m}$ ,  $0.08\text{m}$  and  $0.1\text{m}$ , the results obtained are different.

The same concept applied for Experiment 2 where the inner electrode radius,  $r0$  value is varied. For  $r0= 0.07\text{m}$  and  $0.09\text{m}$ , the sensor does not undergo breakdown because the electrons density is decreased to zero after the simulation begin until the simulation stopped. The sensor breakdown when the simulation is run with  $r0$  value is set to  $0.01\text{m}$ ,  $0.03\text{m}$  and  $0.05\text{m}$ .

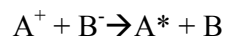
Both experiments share a common factor which leads to the above conditions. The common factor is the space gap or the distance between inner electrodes and outer electrodes,  $d$ . The distance between electrodes is the difference between  $r_1$  and  $r_0$ . The distance is same for both experiments even the value for electrode radius being set is different. The state where the electrons density is decrease to zero is due to the distance between two electrodes is too small and cause electrons lost to the electrodes and to the walls and leave Argon charges only in the region.

There are several processes that lead to the decrease in electrons density:

1. Recombination of positive and negative ions.
2. Three-body recombination of electrons and ions
3. Dissociative recombination.
4. Dielectronic recombination.
5. Electron diffusion.

#### ***4.2.1.1 Recombination of positive and negative ions.***

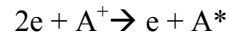
Pairwise recombination of positive and negative ions are described by the relation



The recombination consist of valence electron transferring from the field of atom B to the field of atom  $A^+$ . The process proceeds effectively if the distance between nuclei permits a tunneling transition of the electron [15].

#### ***4.2.1.2 Three-body recombination of electrons and ions***

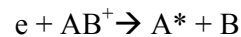
Three-body recombination of electrons and ions process is represented by



This is important for dense plasma. The three-body process produces initially an excited atom whose ionization potential is of the order of thermal energy, and this atom later makes a transition to the ground state as a result of subsequent collisions. Thomson theory is applicable to this process since it involves highly excited atoms [15].

#### ***4.2.1.3 Dissociative recombination.***

Dissociative recombination can be represented by



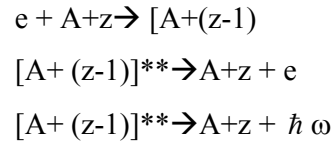
It is a process in which a positive molecular ion is neutralized by recombination with a free electron as a consequence of which the molecule dissociates into two parts [15].

#### ***4.2.1.4 Dielectronic recombination.***

Dielectronic recombination of an electron and ion takes place by capture of the electron into an autoionizing state of the atom and subsequent decay of the autoionizing state by radiative transition to a stable state [15].



This process is important for recombination of electrons and multicharged ions because the radiative lifetime of the multicharged ions decreases strongly with the increase of its charges. This scheme for this process is represented by



#### ***4.2.1.5 Electron diffusion.***

The mechanism of electrons losses is also caused by the diffusional escape of charges towards the discharge chamber walls where they become mutually neutralized, bulk recombination. In electronegative gases, attachment to atoms and molecules form the negative ions [14].

Collisions of excited particles with the walls also lead to the decrease in the number of particles. The efficiency of this process is depending on the identity of the excited particles, the mode of excitation and the properties of the walls [15].

#### *4.2.2 Electrons production*

Electrons and Argon charges density observed to be increased after a certain period. This state is clearly shown in Figure 16, Figure 23 and Figure 28-32 or it can be seen in average density versus time plots for all experiment. This is because of the ionization processes that take place. Lots of electrons are produced from the ionization processes which can be the stepwise ionization and secondary ionization.

At this state, the sensor has reached its minimum breakdown voltage which also known as starting voltage and begins to conduct electricity across the electrodes. Electrons density keeps increasing as the simulation running on and resulted in greater anode current. During this state, the sensor is breakdown and allows current passed through the dielectric medium.

#### *4.2.3 The curvature effect*

The curvature of the sensor is decreased as the radius of the electrodes increased. In general, the curvature of the cylindrical-shaped sensor is the matter of the distance between inner and outer electrode. For Experiment 1, as  $r_1$  changed, distance between two electrodes,  $d$  also changed and the outer electrode curvature also changed. The same concept applied to Experiment 2, as  $r_0$  changed,  $d$  will change and the inner electrode curvature will also change. The similarity and differences between both experiments are shown in Table 9.

Table 9: Comparison between Experiment 1 and Experiment 2

Distance between electrodes, d (m)	Electrodes setting for Exp. 1 (m)	Time taken to breakdown (s)	Average electrons density observed ( $m^{-3}$ )	Electrodes setting for Exp. 2 (m)	Time taken to breakdown (s)	Average electrons density observed ( $m^{-3}$ )
0.01	r0=0.01, r1=0.02	N/A	0	r0=0.09, r1=0.1	N/A	0
0.03	r0=0.01, r1=0.04	N/A	0	r0=0.07, r1=0.1	N/A	0
0.05	r0=0.01, r1=0.06	1.47E-6	4.14E8	r0=0.05, r1=0.1	2.4E-6	4.33E8
0.07	r0=0.01, r1=0.08	1.52E-6	1.52E9	r0=0.03, r1=0.1	1.67E-6	1.61E9
0.09	r0=0.01, r1=0.1	1.53E-6	2.6E9	r0=0.01, r1=0.1	1.53E-6	2.6E9

Table 9 shows that at larger distance between electrodes, average electron density observed during electrical breakdown is higher as compared to the smaller distance between electrodes. As the distance or the gap between inner and outer electrode is increased, electrons needed to create an electrical path in order to conduct electricity across the electrodes will be higher.

For electrodes spacing 0.01m and 0.03m, the electrons density is zero throughout the simulations for both experiments as shown in Figure 16(a)(b) and Figure 23(d)(e). Electrons density observed to be zero between two electrodes at the end of the simulations for 0.01m and 0.03m electrodes gap as shown in Figure 22(a)(b) and Figure 27(d)(e). This happens because of the electrodes spacing is small and leads to a bulky recombination and electrons diffusion to the wall chamber.

#### *4.2.4 Electron mobility*

Before the simulations is started, electrons and Argon charges is in non mobile state. When positive bias is applied to outer electrode, it has become anode and inner electrode is the cathode. When bias applied to the sensor, electric field is applied, the electrons steadily drift in the field direction and because they lose only a small fraction of their energy in elastic collisions with Argon atoms or they rapidly gain energy until they start to undergo inelastic collisions.

The effect of electrons mobility in Argon discharge can be seen in Figure 20 and Figure 25 where the result is obtained after a certain period of simulation. This electrons behaviour will result in collisions and lead to recombination or ionization. Thus, the result obtained is arbitrary and it clearly shows the effect of applying bias to the sensor.

#### *4.2.5 Sheath formation*

In very general terms, plasma bounded by an absorbing wall loses electrons to the wall and shields itself from the resulting electric field by the creation of positive space charge region called sheath. Sheath is a layer in plasma which has a greater density of positive ions, and hence an overall excess positive charge, that balances an opposite negative charge on the surface of a material with which it is in contact. At the edge of bounded plasma, a potential exists to contain the mobile charged species. This allows the flow of positive and negative carriers to the wall to be balanced.

In weakly ionized plasma, the energy to sustain the plasma is generally heating of the electrons by source, while the ions are at near equilibrium with background gas. The electron temperature is typically of few volts, while the ions are cold. In this situation, ions are being accelerated through the sheath while the electrons density decreases according to Boltzmann factor.

The electrons density would then decay on the order of a Debye length. The Debye length is the distance scale over which significant charge densities can spontaneously exist. This resulted in zero electrons density while left behind the Argon charges between electrodes at the end of the simulation. Figure 33 shows the illustration about the sheath form at the wall for both electrodes.

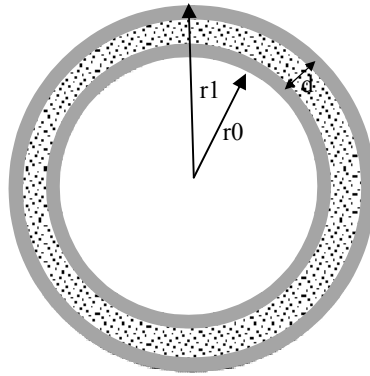


Figure 33: Sheath formed at electrodes wall

The sheath formed at the wall is shown in grey region while the black dots represent the Argon charges. The effect of this sheath form can be clearly observed in Figure 22 and Figure 27. The number of electrons at the sheath region is significantly small as compared to the number of Argon charges at this region.

#### 4.2.6 Sensor breakdown

During the simulation for each experiment, the sensor is breakdown when the average density of electrons is increasing and can be observe from average density plot for each experiment.

For Experiment 1, as the radius of outer electrode increased and moved further from the inner electrode, the time taken for sensor to breakdown is increased and also increased in the average electrons density. However, for Experiment 2, as the radius of inner electrode is increased and moved closer to the outer electrode, the time taken for breakdown to occur is increased but the average electrons density during the breakdown is decreased. Although the electrons density is decreased, it stills higher than the average electrons density for the same electrodes distance in Experiment 1.

This incident is due to the increase in  $r_0$ . Larger  $r_0$  means bigger area of the cathode. Since electrons generated near the cathode, more electrons are produced at cathode, but the electrodes distance became smaller and filled with ions. As electron collide with neutral atom, it produces a negative ion in a process called electron attachment. However, this collision does not produce further electrons by ionization. Thus, the ionization rate will be reduced and caused the time taken for the sensor to breakdown become longer.

The number of electron density is obtained from Equation 2.1 and shows it is dependent on the distance between the electrodes and the Townsend's first ionization coefficient. These factors will influence the number of electrons produced.

As the simulation continues after breakdown is achieved, with electrodes spacing,  $d=0.05\text{m}$ ,  $0.07\text{m}$  and  $0.09\text{m}$ , electrons and Argon charges density is observed to be higher towards the inner electrode. It is shown in Figure 22(c) (d) (e) and Figure 27(a) (b) (c). This happened because inner electrode is configured to be the cathode where free electrons were generated. This also cause by the movement of positively-charged Argon ions towards the cathode. This will cause the density to be higher towards the cathode region.

Close to inner and outer electrode, Argon charges density is higher than electrons density because positive space charge sheath exists. This region is commonly referred as a dark space and caused the excitation rates and visible emission intensities are nearly zero due to the low density and temperature of electrons.

#### *4.2.7 Breakdown voltage*

The analysis about the breakdown behaviour of the cylindrical-shaped ionization gas sensor continues by calculating the breakdown voltage. The breakdown voltage cannot be obtained from the simulation automatically since it has several coefficients and assumption that must be clarified.

Breakdown voltage of gas sensor can be calculated from Equation 2.6. However, the Townsend's second ionization coefficient is unknown, thus the calculation cannot be done unless an assumption about the material used for the electrodes is made. The electrodes are assumed to be carbon electrodes since it is commonly used as electrodes in gas sensing field.

Assuming carbon as the electrodes, Townsend's second ionization coefficient can be calculated by substituting into Equation 2.2 and using reference value of  $r_0=0.01\text{m}$  and  $r_1=0.1\text{m}$  for the radius of the cylindrical electrodes and used to calculate the gap,  $d$ . The pressure is 1torr. The ionization energy of Argon gas and work function of carbon is obtained from Table 1 and Table 2 respectively. Substitute the value into Equation 2.2

$$\gamma_T = (0.016/\text{eV})(I - 2\phi), \quad I = 15.75\text{eV}, \phi = 4.7\text{eV}$$

$$\gamma_T = (0.016/\text{eV})(15.75 - 2(4.7))$$

yield  $\gamma_T = 0.1016\text{eV}$

The coefficient obtained and constant  $C_1$  and  $C_2$  for Argon obtained from Table 3 are substituted into Equation 2.6, yield

$$V_b = \frac{C_2 p d}{\ln\left[\frac{C_1 p d}{\ln(1 + 1/\gamma_T)}\right]}$$

$$C_1 = 12\text{cm}^{-1}\text{torr}^{-1}, C_2 = 200\text{Vcm}^{-1}\text{torr}^{-1}, p = 1\text{torr}, d = 0.09\text{m} = 9\text{cm}$$

$$V_b = \frac{200 * 1 * 9}{\ln\left[\frac{12 * 1 * 9}{\ln(1 + \frac{1}{0.1016})}\right]}$$

$$V_b = 472V$$

Minimum breakdown voltage for the sensor with different electrodes spacing at pressure,  $p=1$  torr are calculated and shown in Table 10.



Table 10: Minimum breakdown voltage for various electrodes spacing  
(Experiment 1,  $r_0$  fixed at 0.01m)

Inner electrode radius, $r_0$ (m)	Curvature, $1/r_0$	Outer electrode radius, $r_1$ (m)	Curvature, $1/r_1$	Electrodes spacing, $d$ (cm)	Minimum Breakdown Voltage, $V_b$ (V)
0.01	100	0.02	50	1	124
0.01	100	0.04	25	3	221
0.01	100	0.06	16.67	5	310
0.01	100	0.08	12.5	7	393
0.01	100	0.10	10	9	472

Table 10 shows that the value of breakdown voltage is different for different values of distance between two electrodes. Equation 2.6 proved that breakdown voltage depends on the product of distance between electrodes and gas pressure. For Experiment 1 and Experiment 2, gas pressure is fixed at 1.0 torr. Other parameters that involve in the calculation such as second ionization coefficient, ionization energy, work function of material,  $C_1$  and  $C_2$  for Argon is obtained from table which is developed by other researchers from their experiments.

For second experiment, the value of outer electrode radius,  $r_1$  is fixed at 0.1m. The breakdown voltage for the sensor is calculated and shown in Table 11.

Table 11: Minimum breakdown voltage for various electrodes spacing  
(Experiment 2, r1 fixed at 0.1m)

Inner electrode radius, r0 (m)	Curvature, 1/r0	Outer electrode radius, r1 (m)	Curvature, 1/r1	Electrodes spacing, d (cm)	Minimum Breakdown Voltage, V <sub>b</sub> (V)
0.01	100	0.10	10	9	472
0.03	33.33	0.10	10	7	393
0.05	20	0.10	10	5	310
0.07	14.29	0.10	10	3	221
0.09	11.11	0.10	10	1	124

The minimum breakdown voltage for gas sensor using carbon as the electrodes at pressure,  $p=1\text{torr}$  is same for both experiments. Minimum breakdown voltage is depends on the distance between two electrodes. As the electrodes spacing increases, the breakdown voltage also increases. Referring to the Paschen's curve for breakdown voltage, the voltage required to transform Argon gas from insulator to become conductor is dependent on the product of pressure multiply with the distance between two electrodes.

Notice that the breakdown voltage is a function of the product  $pd$ . For large value of  $pd$ ,  $V_b$  increases linearly with  $pd$ . For small  $pd$ , there is a minimum breakdown value of  $C_1pd = \ln(1+1/\gamma_T)$  below which breakdown cannot occur. Paschen's curve is a function of the gas and weakly a function of the electrode material.

Breakdown occurs when the electrons are being reproduced rapidly in a electric field. Ionization processes are accompanied by excitations of atoms. Photons generated by radiation from excited particles are absorbed in neighbouring regions and lead to ionization and creation of free electrons. This process will produce more electrons and caused breakdown. Figure 16 and Figure 23 showed the effect of this process. Electrons density observed to be increased after certain period and continue to increase until the simulation is stopped. This showed that breakdown is take place.

#### *4.2.8 Effects of pressure*

The experiment continued with Experiment 3. For this experiment, the electrodes setting is based on Experiment 1 and Experiment 2. Since this experiment is to further investigate the breakdown behaviour of the sensor, the electrodes setting which resulted to the sensor breakdown is chosen. In this case, the electrodes setting for  $d=0.05\text{m}$ ,  $0.07\text{m}$  and  $0.09\text{m}$  for both experiments is set in the input file.

Figure 28 until Figure 32 are the result obtained during the simulation with various pressures. From the result, noticed that the pattern of the plot is almost the same with previous experiment. The density for electrons and Argon charges are higher near the inner electrode. Based on the result obtained, Table 7 and Table 8 are constructed and the average electrons density observed during breakdown appeared to be decreased as the pressure increased.

The time taken for the sensor to breakdown at low pressure as compared to the time taken for the sensor to breakdown at high pressure is increased slightly. At sufficiently high pressure, diffusion processes are retarded because the mobility of the charges is decreased. Argon charges and electrons are largely lost through bulk recombination.

Due to the bulk recombination, longer time is required to produce enough electrons and the ionization rate will be reduced since the mobility is reduced, but the amount of electrons required to initiate breakdown will be less as compared to the breakdown at lower pressure.

When the pressure is low, electrons and Argon charges are lost on the electrodes and walls, not only from bulk recombination. It is because of the diffusion processes. Since electrons and Argon charge mobility is not restricted, the ionization rate is still high as compared to higher pressure; ionization processes will produce electrons rapidly and resulted in higher electrons density during breakdown.

Based on the result obtained from Experiment 3, electrodes setting for  $d=0.09\text{m}$  resulted in fastest response to breakdown. Hence, it became the point of interest for investigating the breakdown voltage for the sensor.

According to Paschen's law, as product of pressure times electrodes spacing,  $pd$  increases, the minimum breakdown voltage will increase. Taking  $r_0=0.01\text{m}$  and  $r_1=0.1\text{m}$  as the electrodes setting, the breakdown voltage is calculated and shown in Table 12 below.

Table 12: Minimum breakdown voltage for various pressures

Pressure, P (torr)	Inner electrode radius, $r_0$ (m)	Outer electrode radius, $r_1$ (m)	Electrodes spacing, $d$ (m)	Breakdown Voltage, $V_b$ (V)
1	0.01	0.1	0.09	472
10	0.01	0.1	0.09	2943
100	0.01	0.1	0.09	21381
1000	0.01	0.1	0.09	167890

From Table 12, a graph of breakdown voltage versus pressure times distance product can be plotted and shown in Figure 28 below.

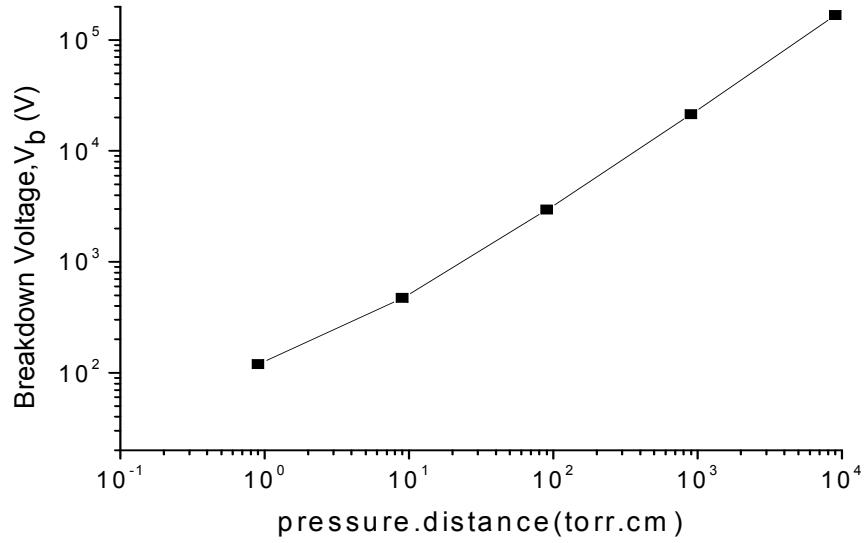


Figure 34: Breakdown voltage Versus Pressure time distance product

Figure 28 shows that breakdown voltage is dependent on the product of pressure and distance as stated is Paschen's law. The graph plotted follows the Paschen's curve for breakdown voltage of Argon gas.

## **CHAPTER 5**

### **CONCLUSION AND RECOMMENDATION**

#### **5.1 Conclusion**

From the result obtained, several conclusions can be made regarding this project. From the simulation done, the breakdown behaviour of the sensor is studied in term of the effect of the curvature to the electrons density and breakdown voltage. Reduces in curvature of the cylindrical-shaped electrodes means increases in the electrodes radius. For instance, as the radius of inner electrode increased, it will be closer to the outer electrode; the distance between two electrodes will decrease.

Smaller distance between electrodes will result in faster response of the sensor to breakdown. However, several criteria should be taking into account before a conclusion could be made. Even though the smaller electrodes distance resulted in faster response of the sensor, it only applied at lower pressure only. Since the pressure is low, the number of electrons generated by diffusion will be greater, but when the pressure is increased, ionization by diffusion became retarded and caused the time taken for the sensor to breakdown increase. Time taken for sensor to breakdown at larger electrodes spacing is reduced at higher pressure. As a result, at higher pressure, the most suitable electrodes setting is  $r_0=0.01\text{m}$  and  $r_1=0.1\text{m}$ .

In order for the sensor to breakdown, the electrons required to create electrical path between electrodes is dependent on the number of ionization processes that take place and the distance between two cylindrical electrodes. For large electrodes spacing, greater number of electrons is required to breakdown the sensor. However, if the electrodes spacing is fixed at certain value and varying the pressure, average electrons density during breakdown is reduced.

Electrons density is observed to be higher at the region closer to the inner electrode since it is generated at the inner electrode. The breakdown voltage of the sensor is dependent on the pressure and the distance between electrodes. For optimizing the sensor performance at high pressure application, the best electrodes setting will be the one with larger electrodes spacing. Hence, the response time for the sensor will be faster and increases its sensitivity.

The objective of this project which is to investigate the curvature effect of cylindrical-shaped ionization gas sensor and to investigate the breakdown behaviours of ionization gas sensor is achieved.

## **5.2 Recommendation**

The sensitivity of the sensor can be optimized by optimizing the shaped of the sensor. However, the sensor's performance can be further improved in terms of their selectivity to various gases. Further study and research should be commenced about this issue in order to improve the overall performance of ionization gas sensor.

## REFERENCES

- [1] "How Smoke Detectors Work." 01 April 2000. HowStuffWorks.com.  
<http://home.howstuffworks.com/home-improvement/household-safety/fire/smoke.htm>
  
- [2] Ramin Banan Sadeghian and Mojtaba Kahrizi, 2007, *A Low Voltage Gas Ionization Sensor based on Sparse Gold Nanorods*, Canada, Concordia University.
  
- [3] Salman Mahmood, Zainal Arif Burhanudin, and Nor Hisham Hamid, *Simulation of Electron Densities and Breakdown Voltages in Argon-Filled Cylindrical Electrodes*, Department of Electrical & Electronic Engineering, Universiti Teknologi PETRONAS, 31750 Tronoh, Perak, MALAYSIA.
  
- [4] "What is MEMS Technology?" MEMS and Nanotechnology Exchange.  
<<https://www.memsnet.org/mems/>>
  
- [5] "Operating Principle." 2008. FIGARO Engineering Inc.  
< <http://www.figaro.co.jp/en/item2.html> >
  
- [6] N B^arsan and UWeimar, *Understanding the fundamental principles of metal oxide based gas sensors; the example of CO sensing with SnO2 sensors in the presence of humidity* Institute of Physical and Theoretical Chemistry, University of T^ubingen, Auf der Morgenstelle 8, D-72076 T^ubingen, Germany.



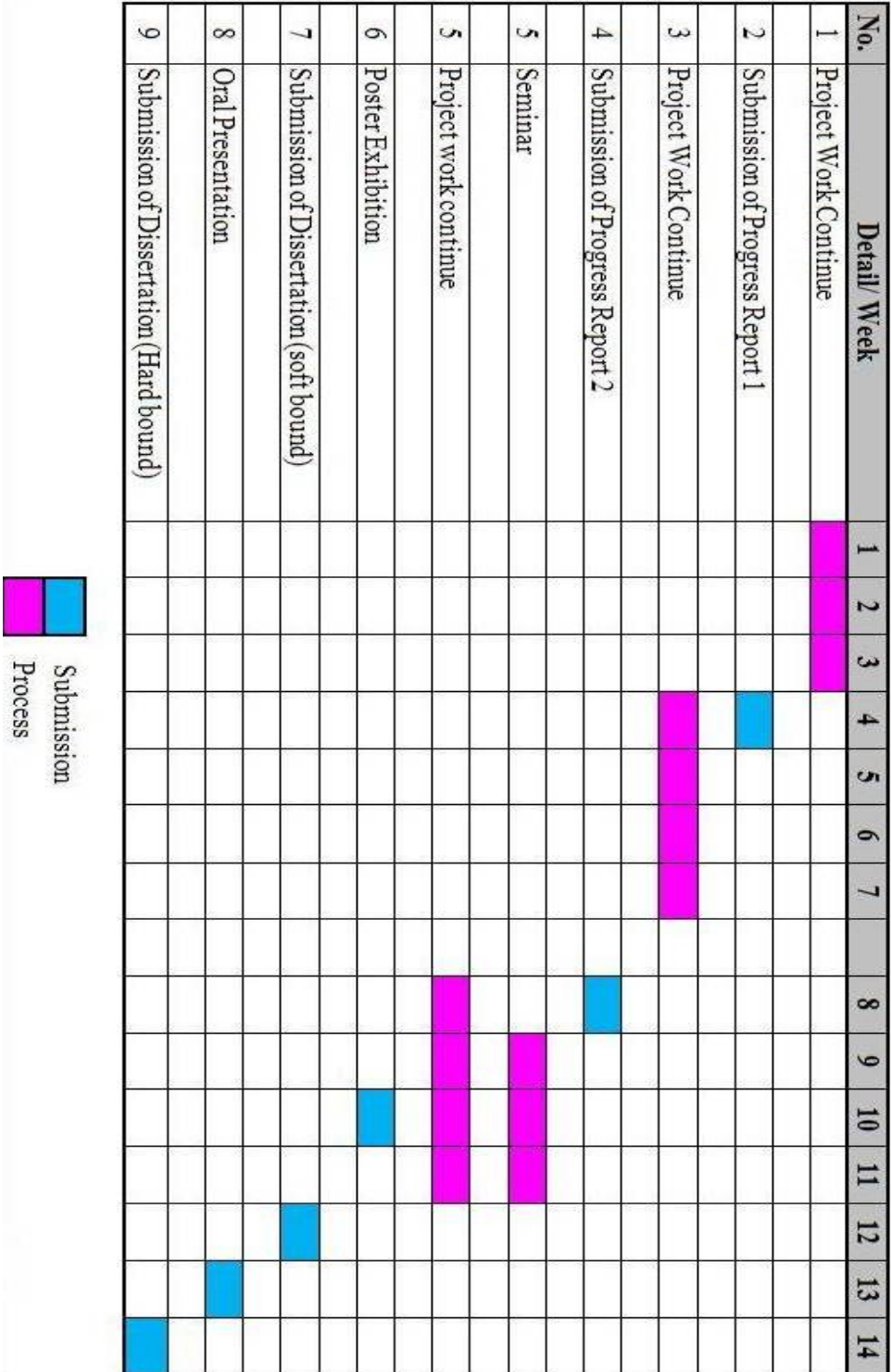
- [7] K. Arshak, I. Gaidan, *Development of a novel gas sensor based on oxide thick films*, Microelectronic and Semiconductor Research Group, Electronic and Computer Engineering Department, University of Limerick, Plassey Technological Park, Limerick, Ireland.
- [8] "Ions and Ionization." 01 July 2009. HowStuffWorks.com.  
<<http://science.howstuffworks.com/ions-and-ionization-info.htm>>
- [9] Sayed Saad. 27 May 2006  
<[http://www.sayedsaad.com/High\\_voltge/index\\_gasses.html](http://www.sayedsaad.com/High_voltge/index_gasses.html)>
- [10] Mitsuharu Konuma, *Plasma Techniques for Film Deposition*, Alpha Science International Ltd, Harrow, UK, 2005.
- [11] Declan A Diver, *A Plasma Formulary for Physics, Technology and Astrophysics*, Wiley-VCH Verlag Berlin GmbH, Berlin, Germany, 2001.
- [12] Larry K. Warne and Roy E. Jorgenson, *Ionization Coefficient Approach to Modeling Breakdown in Nonuniform Geometries*, Sandia National Laboratories, Albuquerque, New Mexico 87185 and Livermore, California 94550.
- [13] Peter Dunsby, Mon Sep 16 1996  
<<http://www.mth.uct.ac.za/omei/gr/chap6/node8.html>>
- [14] Yuri P. Raizer, Mikhail N. Shneider, Nikolai A. Yatsenko, *Radio-Frequency Capacitive Discharges*, CRC Press LLC, 1995.
- [15] Boris M. Smirnoz, *Physics of Ionized Gases*, John Wiley & Sons, Inc, Canada, 2001.
- [16] Laaknor. 23 January 2010. Wikimedia Foundation Inc  
<[http://en.wikipedia.org/wiki/Townsend\\_discharge](http://en.wikipedia.org/wiki/Townsend_discharge)>
- [17] 5 Oct 2009. Mc Graw-Hill Concise Encyclopedia of Physics.  
<<http://encyclopedia2.thefreedictionary.com/breakdown+potential>>

- [18] Shaddack. 18 April 2010.  
< [http://en.wikipedia.org/wiki/Paschen%27s\\_law](http://en.wikipedia.org/wiki/Paschen%27s_law)>
- [19] Plasma Theory and Simulation Group, *1-dimensional Electrostatic Plasma Device Cylindrical (XPDC1) manual*, EECS Department, University of California, Berkeley, CA 94720.
- [20] Plasma Theory and Simulation Group, *1-dimensional Electrostatic Plasma Device Planar (XPDP1) manual*, EECS Department, University of California, Berkeley, CA 94720.

## **APPENDICES**

## APPENDIX A

**Gantt Chart**



## APPENDIX B

### Input file for simulation

```
Breakdown of an argon discharge

-nsp---nc--grid--nc2p---dt[s]-----r0[m]----r1[m]---height[m]--epsilon--
Bz[Tesla]-
  2    500  1    1e4    5e-10    0.01    0.10    0.145    1.0    0.0

-rhoback[C/m^3]-backj[Amp/m^2]---dde---extR[Ohm]--extL[H]---extC[F]--q0[C]-
  0.0    0.0    0.0    0.0    0.0    2e-11    0.0

-ramped--source--dc[V|Amp]--ramp[(V|Amp)/s]--ac[V|Amp]--acramp[s]--f0[Hz]--
theta0[D]-
  1          v    0.0    0.0    250.0    1.0e-6    1.36e7    0.0

--secondary----e_collisional----i_collisional----reflux----nfft--nsmoothing--
RT_flag--
  0          1          2          0    512    10    0

--seec(electrons)---seec(ions)---ion species----Gpressure[Torr]---GTemp[eV]--gas
  2.4    0.2    2          1.0    .026    1

SPECIES 1

----q[C]-----m[Kg]---j0L[Amp/m^2]---j0R[Amp/m^2]----initn[m^-3]--prof--sp_k
-1.602e-19  9.11e-31    0.0    0.0    1e10    1    1

--v0L[m/s]---v0R[m/s]---vtL[m/s]---vtR[m/s]----vcL[m/s]---vcR[m/s]--
  0.0    0.0    1e6    1e6    0.    0.

--v0t[m/s]---vtt[m/s]---v0z[m/s]---vtz[m/s]--
  0.0    1E6    0.0    1E6

---nbin----Emin[eV]----Emax[eV]---max-np---
  50    0    100    40000

-For-Mid-Diagnostic---nbin----Emin[eV]---Emax[eV]----XStart--XFinish--
  200    0.0    20.0    0.0008    0.0010

-For-vel_dist---vx_lower--vx_upper--nxbin--vy_lower--vy_upper--nybin--vz_lower-
  -3.0e6    3.0e6    0    -3.0e6    3.0e6    0    -3.0e6

  vz_upper--nzbin-
  3.0e6    0

SPECIES 2

----q[C]-----m[Kg]---j0L[Amp/m^2]---j0R[Amp/m^2]----initn[m^-3]--prof--sp_k
  1.602e-19  6.69e-26    0.0    0.0    1e10    1    1

--v0L[m/s]---v0R[m/s]---vtL[m/s]---vtR[m/s]----vcL[m/s]---vcR[m/s]--vtperp[m/s]--
  0.    0.    7e2    7e2    0.0    0.0    7e2

--v0t[m/s]---vtt[m/s]---v0z[m/s]---vtz[m/s]--
  0.    7e2    0.    7e2

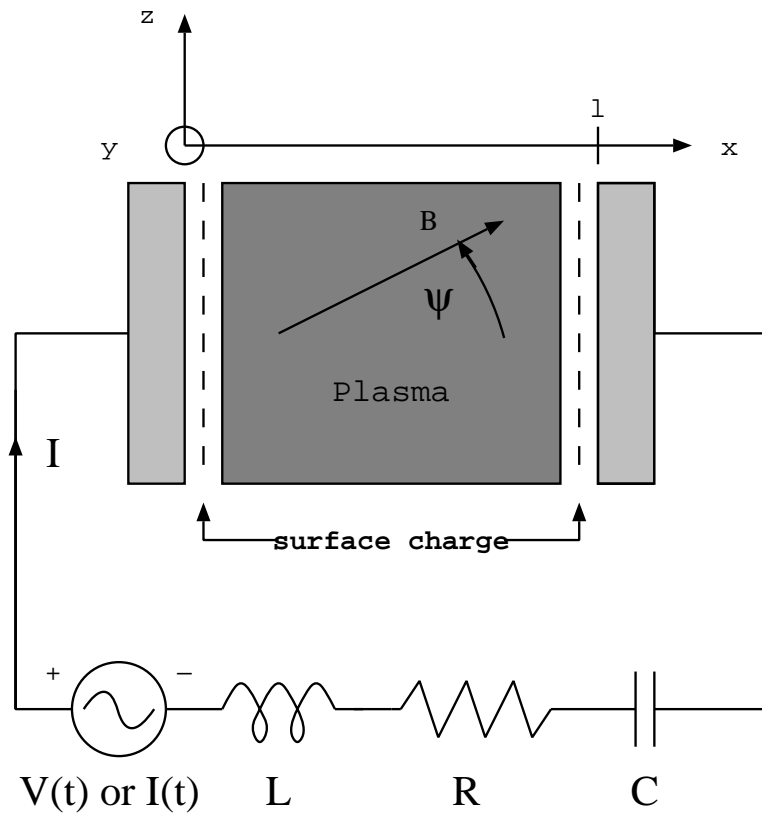
---nbin----Emin[eV]----Emax[eV]---max-np---
  50    0    50    40000

-For-Mid-Diagnostic---nbin----Emin[eV]---Emax[eV]----XStart--XFinish--
  200    0.0    2    .0    .0002

-For-vdf--vr_low--vr_up--nrbin--vt_low--vt_up--ntbin--vz_low--vz_up--nzbin-
  -1.0e3    1.0e3    0    -1.0e3    1.0e3    0    -1.0e3    1.0e3    0
```

## APPENDIX C

### XPDC1 Manual



PDC1

# Cylindrical Plasma Device 1 Dimensional Bounded Electrostatic Code

Plasma Theory and Simulation Group  
EECS Department, University of California,  
Berkeley, CA 94720

# Contents

<b>1</b>	<b>INTRODUCTION</b>	<b>4</b>
1.1	Scope . . . . .	4
1.2	Interface with graphics . . . . .	5
<b>2</b>	<b>INSTALLATION</b>	<b>7</b>
2.1	Setup and Installation Procedure (X Windows version) . . . . .	8
2.2	Installation Procedure (Parallel Version) . . . . .	8
2.2.1	Download and install MPI . . . . .	8
2.2.2	Download and install latest XGrafix library . . . . .	10
2.2.3	Download and install parallel XPDC1 . . . . .	10
2.2.4	Syntax for running Parallel XPDC1 . . . . .	11
2.3	Instructions for using power balance module . . . . .	12
<b>3</b>	<b>X-WINDOWS PROGRAM OPERATION</b>	<b>14</b>
3.1	Syntax . . . . .	14
3.2	GUI Support . . . . .	14
3.3	Main Menu . . . . .	14
3.4	Diagnostic Window Buttons . . . . .	15
3.4.1	Rescale . . . . .	15
3.4.2	Trace . . . . .	15
3.4.3	Print . . . . .	15
3.4.4	Crosshair . . . . .	15
3.5	Diagnostics . . . . .	15
<b>4</b>	<b>INPUT FILES</b>	<b>16</b>
4.1	Input File Parameters . . . . .	16
4.1.1	Global Parameters . . . . .	16
4.1.2	Applied Voltage Or Current Sources . . . . .	17
4.1.3	Flags . . . . .	20
4.1.4	Wall Emission Coefficients and Neutral Gas Parameters	21
4.1.5	Electron-Neutral Cross-sections . . . . .	21
4.1.6	Ion-Neutral Cross-sections . . . . .	25



4.1.7	<b>Species Parameters</b>	25
4.2	<b>Radiation transport Parameters</b>	30

# 1 INTRODUCTION

XPDC1 is a bounded electrostatic code for simulating a 1 dimensional plasma discharge, running on Unix workstations with X-Windows, and PC's with an X-Windows emulator. The code simulates a bounded cylindrical dc discharge with a the characteristics of which are specified by the user at run time using an input file. The discharge power comes from an axial source, and can be specified as one of an axial electric field, discharge current or power. The source is made general so that it can be AC or DC, and ramped with a specified time constant. The simulation can proceed in real-time, with the user viewing output as the code runs in the form of various user specified diagnostics which are updated each time step (animation). To improve run times, or to run in batch mode, the simulation can be run without graphics, which means that most of the diagnostics are not calculated.

The code compiles with standard C compilers and requires X-Windows libraries (X10 or higher).

## 1.1 Scope

This document describes the XPDC1 programs running on the workstations and UNICOS Cray environment. The general physics issues involved in a bounded plasma simulation are discussed briefly. Program installation, operation, and modification are discussed. In addition, the library of input files accompanying XPDC1 is described, and the guidelines to generate new input files are provided.

This manual makes no attempt to explain exhaustively the physics and computational issues of particle simulation. Many comprehensive texts on particle simulation are available [1] [2].

Some familiarity with plasma physics is required to understand the results of the simulations and generate new simulations. Knowledge of numerical analysis and/or particle simulation is useful for modification of the code and understanding of numerical errors which can occur in any computer simulation.

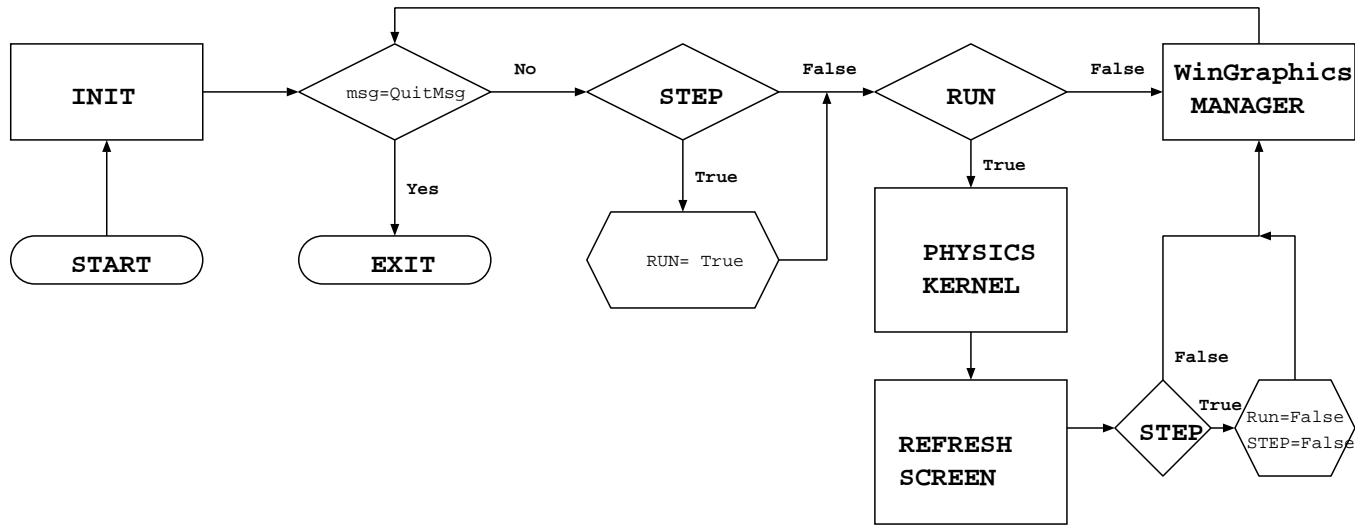


Figure 1: Schematic representation of the interaction between WinGraphics and the physics kernel.

## 1.2 Interface with graphics

The code is separated into a physics application and the windowing core as shown in Figure 1. New physics and diagnostics can be added without altering the windowing code, with the only restriction that any new diagnostic must be a linear, semi-log, or scatter plot. A text plot is currently under consideration which would display parameters from the input file during the simulation.

Using the windowing core, all diagnostics are updated dynamically in time. The core can also update in individual time-steps, pausing for a keystroke before continuing the simulation.

The code runs significantly faster when fewer (or zero) plots are displayed on screen. Therefore, when output is not being viewed (long runs overnight, coffee break, etc.), it is more efficient to remove all plots from the screen.

All time histories are combed periodically such that there are never more than HIST-MAX (a programmable constant) values stored. Note that after long runs this can result in a loss of high frequency resolution on the time history plots. This has no

effect on the physics of the simulation since the diagnostics are simply a view of the physical results.

PDC1 can generate output in either eps, xgm, gif, ascii (data) or xgbin formats. The resolution and grey-shading of the output is dependent only on the output device.

PDC1 employs 7 circuit solvers to handle the full range of external circuit parameters. The general voltage-driven series RLC case is solved using a second order backward Euler method. For the open circuit case,  $C \rightarrow 0$ , the external circuit no longer needs to be solved; the boundary surface charge influences the potential as always, but it cannot exchange charge (via current) with the other boundary. For  $C \rightarrow \infty$  and  $R = L = 0$ , the external circuit becomes a short circuit, so the applied potentials are applied directly to the plasma boundaries. The final case is an ideal current source, which imposes the specified current independent of the external circuit parameters or boundary potentials. For a complete discussion of the simultaneous solution of the external circuit and the spatial plasma potential, refer to the attached paper[5].

FFT routines are used to transform time histories into frequency domain plots. Both amplitude and phase of the transformed quantity are available. This feature is useful when looking for response of a bounded plasma at one or more frequencies, as well as determining the impedance of the plasma to external currents/voltages.

## 2 INSTALLATION

This section describes the contents of the XPDC1 distribution and its installation procedure.

The codes are available in the tar gzipped form from the **PTSG** web site at <http://ptsg.eecs.berkeley.edu>. **xgrafx** distribution is available separately at the same web site and has to be installed for any of the PTSG family of codes to work. The contents of the XPDC1 distribution contains:

README.parallel	Text file containing the direction for installing the parallel version of XPDC1, including installing MPI libraries.
README.powBal	Text file containing instructions for installing the power balance module
XPDC1.TAR	The tar file containing the files required for XPDC1.

**\xpd1\src** directory:

\*.c All files with the .c extension are the C language source files for XPDC1. These files should be placed in the xpd1/src directory.

.h All files with the .h extension are the C language header files for XPDC1. These files should be placed in the xpd1/src directory.

makefile The make file for automatically performing conditional compilation /linking of only those files which have been changed. This file should be placed in the xpd1/src directory.

par.sh extension: compiles and links the parallel version of the code, for dual processor sharing on the same machine

par.p4 extension: compiles the parallel version, for sharing 4 processors over the network

**\xpd1\inp** directory:

\*.inp All files with the inp extension are input files. For detailed information on each input file refer to Section 4.2 Input File Library.

A directory called inp is set up under the xpd1 directory to include all the input files.

The **xgrafx** distribution contains the required files for displaying graphics in the X Windows version. These are:

- |            |  |
|------------|--|
| README     | Text file containing some directions and information on compiling the XGrafix libraries. When the information in this manual conflicts with the README file, assume the file is correct. |
| xgrafx.c   | The source file for the XGrafix graphics display library. This file should be placed in the xgrafx directory.  |
| xgrafx.h   | Header file for XGrafix. This file should be placed in the xgrafx directory.   |
| xgrafx.ico | The XGrafix icon (bitmap). This file should be placed in the xgrafx directory.   |
| xgrafx.str | Another header file containing string definitions for XGrafix. This file should be placed in the xgrafx directory.   |
| makefile   | The make file for XGrafix. This file should be placed in the xgrafx directory.   |

## **2.1 Setup and Installation Procedure (X Windows version)**

The installation procedure to a workstation must be done manually. Take the tar file along with the README file to your workstation or Unix platform. Follow the directions in the README file for installation and compiling. Read the README file in the xgrafx directory as well as the makefile before compiling XGrafix, then compile xpdc1.

## **2.2 Installation Procedure (Parallel Version)**

### **2.2.1 Download and install MPI**

The first step in using the parallel version of XPDC1 is to download and install the MPI libraries on your system.

1. Go to the website <http://www-unix.mcs.anl.gov/mpi/mpich/> and download the file `mpich.tar.gz` which contains the MPICH portable implementation of MPI. You can also read the Installation Guide and User's Guide at this site in HTTP format.
2. `gunzip` the file and `unarchive` it, you will then create a directory called `mpich-1.2.0` (or the name of the current version).
3. For version 1.2.0 compiling on a LINUX machine, use the following steps to compile and install MPICH: Enter the `mpich-1.2.0` directory, then type
  - (a) `configure --with-device=ch_p4 -rsh=ssh`
  - (b) `make`
  - (c) `make install PREFIX=/usr/local/mpich-1.2.0`

In step (a), MPI is configured with the `ch_p4` device which assumes a default network and makes no assumption about memory sharing.

If your system is configured to use the secure shell `ssh`, you should also use the option `"-rsh=ssh"`; otherwise, omit this option.

To see all the configuration options, type `"configure -usage"`.

In step (b), the code is compiled and in step (c), it is installed to the directory `/usr/local/mpich-1.2.0`. You may choose another installation directory. Also note that you must be root to install to a system directory.

4. Next you may also wish to install the shared memory MPI (`ch_shmem`) library. If you do not, skip this section.

For version 1.2.0 compiling on a LINUX machine, the following steps are used to install the `ch_shmem` MPI library:

First copy the `mpich-1.2.0` directory to `mpich-1.2.0sh`. Enter the `mpich-1.2.0sh` directory and type:

- (a) `make clean`
- (b) `configure --with-device=ch_shmem -rsh=ssh`

(c) make

(d) make install PREFIX=/usr/local/mpich-1.2.0sh

In step (a), any object files left over by a previous installation are cleaned up. In step (b), MPI is configured with the `ch_shmem` device which assumes a shared memory (SMP) configuration. Also, as mentioned before, if your system is not configured to use the secure shell `ssh`, omit the second configuration option. In step (c), the code is compiled, and in (d) the library is installed in `/usr/local/mpich-1.2.0sh`. As mentioned before, you may choose another directory, and you must be root to install to a system directory.

### 2.2.2 Download and install latest XGrafix library

Obtain the latest version of XGRAFIX from our CVS repository. This version has minor revisions to enable the parallel version of XPDC1 to work.

1. First edit the `Imakefile` by UNcommenting the line: `MPI_DEFINE = -DMPI_1D`
2. Type “`xmkmf`” to create the `Makefile`.
3. Type “`make`” to create the library `libXGC250.a`
4. Rename `libXGC250.a` to `libXGC250P.a`, and move it to the library where you keep all other `xgrafx` libraries, e.g., `/usr/local/lib/xgrafx`.
5. Finally, replace the old “`xgrafx.h`” in `/usr/local/include` (or wherever it resides) with the current version of `xgrafx.h`

### 2.2.3 Download and install parallel XPDC1

Obtain the latest version of XPDC1 from our CVS repository. This includes the parallel version of XPDC1.

1. First read `makefile.par.p4`, and edit the file so that all the directory locations are correct.



2. Next type: “make -f makefile.par.p4” This will create the executable “xpdcl.par.p4” which uses the default network (ch\_p4) MPI library.

If you have installed the shared memory (ch\_mem) library, and wish to create an executable which uses this library, then,

3. read makefile.par.sh, and edit the file so that all the directory locations are correct.
4. type: “make -f makefile.par.sh” This will create the executable “xpdcl.par.sh” which uses the ch\_mem library.

#### 2.2.4 Syntax for running Parallel XPDC1

After completing installation instructions you are now ready to use parallel xpdcl (n.b., code can only be run in parallel **without** Xgrafx (i.e., diagnostics will not be available). Therefore it is best to run the parallel code in background for longer runs (say to achieve equilibrium) and then run in single processor mode to examine the results.

1. CH\_P4 version:

- (a) Let `$(DEST_P4) = <$Location of ch_p4 MPI library>$.` (For the example in 2.2.1, `$(DEST_P4)=/usr/local/mpich-1.2.0`).

- (b) Check the file `$(DEST_P4)/share/machines.LINUX` to make sure the information is correct.

- (c) Type,

```
$(DEST_P4)/bin/mpirun -np <num proc.'s> xpdcl.par.p4 -i <inputfile>  
-dp <dump period> -d <dumpfile> -s <num. steps> -nox
```

If you do not wish to use the default machines listed in

```
$(DEST_P4)/share/machines.LINUX, the mpirun command has an option  
“-machinefile <your machinefile>”.
```

2. CH\_SHMEM version:

- (a) Let `$(DEST_SH) = <Location of ch_mem MPI library>.` (For the example in I, `$(DEST_SH)=/usr/local/mpich-1.2.0sh`)

- (b) Type, `$(DEST_SH)/bin/mpirun -np <num proc.'s> xpdc1.par.sh -i <inputfile> -dp <dump period> -d <dumpfile> -s <num. steps> -nox`

### 3. NOTES

- (a) Current version of Parallel XPDC1 requires you to use the `-nox` option with number of steps and dump period specified. It also assumes that you are starting a simulation from a dump file. If you do not have a dump file, generate one by running the non-parallel XPDC1 for a few timesteps and saving the result.
- (b) Input files and dump files are fully compatible between the parallel and non-parallel versions.
- (c) To observe diagnostics, start a non-parallel `xpdc1` with `X` turned on with a dumpfile generated from the parallel version.

## 2.3 Instructions for using power balance module

In order to use the power balance module, which calculates nett power gains and losses in a positive column discharge, you must edit the relevant makefile (`makefile`, `makefile.par.p4`, `makefile.par.sh`) so that the line `"DEFINES = -DPOW"` is uncommented before compiling the code.

If you do this, then every `POW_DT` timesteps, XPDC1 will dump the power and particle balance information into an ascii file with the suffix `".dmp.pow"`. `POW_DT` is currently set to 10000 timesteps. However, you can change this by editing the line `"#define POW_DT 10000"` in the file `"pdc1.c"`.

An example of the output from the code running on the reduced problem ( $E_z = 100$  V,  $I_{in} = 15.2$  mA,  $h = 20$  cm,  $R=1$ cm,  $p=2.83$  mTorr) looks as follows:

```
time = 1.680000e-05
species=0, particle loss to wall =2.2049e+10
species=1, particle loss to wall =2.19716e+10
number of ionization events =2.1928e+10
species=0, power loss to wall = 0.0670558 W
species=1, power loss to wall = 0.118345 W
```

power loss to inelastic colls = 0.10719 W  
power loss to elastic colls = 6.18593e-05 W  
power loss to charge exchange colls = 0.00936686 W  
total power loss to colls = 0.116619 W  
total power loss to wall = 0.185401 W  
total power loss = 0.30202 W  
power Input = 0.300904 W

Here, species 0 is the electron, and species 1 are the Ar+ ions. Note that the simulation has reached equilibrium since the particle loss to the wall for each species in POW\_DT timesteps is equal to the number of ionization events in POW\_DT timesteps. Also the total power loss equals the power input ( $E_z * I_z * h$ ).

The power balance module assumes a positive column discharge. So, you may want to suppress it by commenting it out of the relevant makefile if you are simulating other types of discharges.

## **3 X-WINDOWS PROGRAM OPERATION**

### **3.1 Syntax**

```
xpdc1 -i filename[.inp] -d [dumpfile.dmp]
```

where < filename.inp > is the name of the input file. Although we have used \*.inp for the input files in the library, the .INP extension is not required. If no filename is provided on the command line, XPDC1 displays an error message. The dumpfile parameter is optional; it must be an existing file created by the same version of the code. If the input files are not in the same directory or are located in a sub-directory, the path must also be specified. For instance, the syntax for starting XPDC1 with the input file vc.inp which is in a sub-directory of xpdc1 called inp is:

```
xpdc1 -l inp/vc
```

The input file is required since XPDC1 determines the parameters of the simulation at run time.

### **3.2 GUI Support**

XPDC1 fully supports a mouse for selection of items, buttons etc. Moving, resizing, and iconifying of windows is supported indirectly via the X window manager (Motif, Open Look, etc.). Keystrokes are not supported for these actions, so a mouse is required. The move, resize, and iconifying buttons and operations are governed by the window manager; consult the window manager manual or guru for details of these procedures.

### **3.3 Main Menu**

The buttons on the main menu can be selected using the mouse. The functions available include RUN, STOP, STEP, SAVE, and QUIT, which all perform the same function described previously in Section 3. Note that the SAVE function is equivalent to the DUMP function in the MS-DOS version which is also NOT implemented in this version.

## **3.4 Diagnostic Window Buttons**

Every diagnostic window in XPDC1 contains four buttons: Rescale, Trace, Print, and Cross-hair.

### **3.4.1 Rescale**

The rescale button pauses the simulation and opens a dialog box containing editable fields for the minimum and maximum labels on the x and y axes. In addition, the dialog box contains buttons for automatic rescaling of the x and y axis. These buttons toggle auto rescaling of the respective axis on and off. When all axes are scaled as desired, select OK to accept the changes or CANCEL to return to the previous status. Note that while rescaling the simulation is paused.

### **3.4.2 Trace**

The trace button turns toggles the plot tracing feature on and off. The previous plots are accumulated, generating a series of lines or dots as described above.

### **3.4.3 Print**

The Print button generates a PostScript plot file of the current window. Pressing the button opens a dialog box containing the file name for the plot and a plot title. Selecting OK generates the plot, CANCEL returns to the simulation. Note that the simulation is paused while the dialog box is open.

### **3.4.4 Crosshair**

The crosshair button activates the crosshair pointer and opens a dialog box displaying the coordinates of the pointer. To display the coordinates of a point move the crosshair pointer to the desired location and click. The simulation is paused until the crosshair is deactivated by selecting the Crosshair button again.

## **3.5 Diagnostics**

A list of available diagnostics is produced when the simulation is run with Xgraphics (the default condition) Clicking on the diagnostic name will produce a plot window.

## 4 INPUT FILES

XPDC1 obtains its versatility through the use of input files. The input file contains the parameters for the simulation, specifying number of each species, grid spacing, charge to mass ratios, etc. This section describes the contents, use, and modification of input files for XPDC1.

### 4.1 Input File Parameters

The codes use input files to describe the simulation, including the physical bounded device parameters, external circuit, RF drive, etc. (global parameters), as well as the parameters describing each species of particles. Units, if any, are shown in [ ].

#### 4.1.1 Global Parameters

nsp	The number of particle species to simulate (0= no species present, may use this option to check the system, 1= one species in the whole system, etc.). If modifying an input file that has, say, 2 species, to add more species, just copy one of the blocks of parameters corresponding to species 1 or 2, and change the parameters to the desired values. Note that each species added requires a substantial increment in memory.
nc	The number of spatial cells. For a uniform grid the cell width is calculated using $\Delta r = r_1/nc$ , for the non-uniform grids the calculation is more complicated.
grid	flag for type of grid spacing 0: constant volume mesh 1: uniform mesh 2: linearly decreasing mesh 3: uniform mesh with a change in grid spacing at $r_1/2$
nc2p	The number of physical particles per computer particle. The number of super particles in the simulation is found using $N = initn \cdot \pi \cdot r_1^2 h / nc2p$ , where $initn$ is the uniform number density.

dt	The time step [sec].
r0	Inner electrode radius[m].
r1	Outer electrode radius[m].
height	Axial length of cylinder [m]. Allows application of real currents and real external circuit parameters.
epsilon	Background relative dielectric constant of system.
B	Applied axial magnetic field ( $B_z$ ) [Tesla].
rhoback	Fixed background charge density (non-accelerating) [C/m <sup>3</sup> ].
backj	Background current density (non-accelerating) [Amps/m <sup>2</sup> ].
dde	Sinusoidal perturbation of charge density ( $\delta r/l$ ) at $t = 0$ ; $\delta r(x) = l \cdot dde \cdot \sin(2\pi x/l)$
extR	External circuit resistance [Ohms].
extL	External circuit inductance [Henries].
extC	External circuit capacitance [Farads].
q0	Initial capacitor charge [C].

#### 4.1.2 Applied Voltage Or Current Sources

When the flag dcramped is off, the general form of the applied source is:

$$S(t) = DC + Ramp \cdot t + AC \cdot \sin(2\pi f_0 t + \theta_0)$$

where  $S(t)$ , the applied source, is either a current or a voltage source.

The flag `dcramped` should be turned on (set to 1) when a step function is desired. The step function can have a zero rise time,  $Ramp \gg 1$ , or can be ramped to its final DC value with a constant slope.

<code>source</code>	With an inner electrode this specifies either a voltage or current source: V=voltage I=current When there is no inner electrode, it specifies an axial source term: P - axial power source I - axial current source E - the axial electric field is specified directly
<code>dcramped</code>	Flag for ramping source to a final DC value (1=yes, 0=no).
<code>DC</code>	DC external voltage or current source [V, Amps]; or axial power, current or electric field [Watts, Amps, V/m]. Zero value indicates zero dc voltage.
<code>Ramp</code>	Rate of ramping for voltage or current source [V/sec or Amps/sec]. Zero value indicates zero ramping for voltage.
<code>AC</code>	AC voltage or current source [V or Amps]; or axial power, current or electric field [Watts, Amps, V/m]. Zero value indicates zero ac voltage and the values of $f_0$ and $theta_0$ are ignored.
<code>f0</code>	AC source driving frequency [Hz].
<code>theta0</code>	Initial phase angle of AC source [deg].



### Axial field calculation

For an axial current source, the axial electric field is calculated from

$$I_z = 2\pi \int_0^R J_z(r) r dr = 2\pi e \int_0^R n_e(r) \mu_e(r) E_z(r) r dr$$

where

$$\mu_e = \frac{e}{m_e \nu_m}$$

is the electron mobility and  $\nu_m$  is the electron-neutral collision frequency. The average collision frequency is calculated by summing over the distribution function.

$$\nu_m = N_g \langle \sigma v \rangle = N_g \frac{\sum_{i=0}^{N_e} \sigma_m(v_i) v_i}{N_e}$$

where  $\sigma_m$  is the momentum transfer cross-section,  $v$  is the electron velocity,  $N_g$  is the background gas density and  $N_e$  is the number of electrons in the simulation. Presuming the axial electric field and the mobility have little radial variation  $E_z$  can be calculated from

$$E_z = \frac{I_z}{2\pi e \mu_e \int_0^R n_e(r) r dr} = \frac{h I_z}{e \mu_e N_e}$$

For an axial power source, the axial electric field is calculated from

$$P_z = E_z h I_z$$

where  $h$  is the axial length of the cylinder. The axial current is calculated from

$$I_z = 2\pi \int_0^R J_z(r) r dr = 2\pi e \int_0^R n_e(r) \bar{v}_z(r) r dr$$

where  $\bar{v}_z$  is the drift velocity in the axial direction. Assuming that this is radially independent it is calculated by averaging over the electron axial velocities

$$\bar{v}_z = \frac{\sum_{i=0}^{N_e} v_z}{N_e}$$

Then

$$E_z = \frac{P_z}{\bar{v}_z N_e}$$

### 4.1.3 Flags

secondary	Secondary electron emission flag (0=off, 1=species 1 emitted, etc.). The emitted electron species give the emitted velocity distribution at the surface specified for the species (see SPECIES PARAMETERS).
e_collisional	The flag for ionization, elastic, and excitation electron-neutral collisions (0 = off, 1 = species 1 is the colliding electron species, etc.). Note: Only ONE species can be the colliding electron species.
i_collisional	The flag for scattering and charge exchange ion-neutral collisions (0 = off, 2 = species 2 is the colliding ion species, etc.). Note: Only ONE species can be the colliding ion species.
reflux	The flag for refluxing the particles at the outer wall (0=off, 1=on). In this case, the particles hitting the outer wall are not absorbed but reflected back into the system. Since the outer wall in this case does not charge up, it serves only as a symmetry plane allowing for a semi-infinite plasma at the right wall. The particles of each species are refluxed at the temperature specified for the species.
nfft	Number of samples for the Fast Fourier Transform analyzer (must be a power of 2). When this parameter is set to zero, no FFT analysis is done, and the diagnostics in the frequency-domain are NOT shown.
n_ave	Number of samples for the average diagnostics. When this parameter is set to zero, no averages are not done and NOT shown.
nsmoothing	Number of time that a (1, 2, 1) digital smoothing filter is applied to the charge density arrays prior to the field-solve.
RT_flag	Flag specifying whether radiation transport module is used (0=off 1=on).

#### 4.1.4 Wall Emission Coefficients and Neutral Gas Parameters

seec(elect.)	The coefficient of secondary electron emission due to the first species striking the electrode(s). If this parameter is set to say 0.1, on average one electron is injected for every 10 incident particles of this species.
seec(ions)	The coefficient of secondary electron emission due to the second species striking the electrode(s).
ion species	indicates the ion species created by electron-neutral ionization collisions (2=the created ions are of type species 2, etc.). Note: this also specifies the type of the background neutral gas particles colliding with electrons.
Gpressure	Background neutral gas pressure [Torr].
Gtemp	Background neutral gas thermal temperature [eV].
GAS	Type of cross-sections used in the simulation. GAS = 1 - e-Ar cross-sections using curve fits from paper by Lawler and Kurtshagen [12], and Ar <sup>+</sup> -Ar from hbs cross-section fits. GAS = 2 - e-Ar and Ar <sup>+</sup> -Ar cross-sections using curve fits by H.B. Smith and anisotropic electron scattering.

#### 4.1.5 Electron-Neutral Cross-sections

##### HBS Cross-sections

The cross-section curve fits (shown in Figure 2) have the form

*Ionisation*

$$\sigma_{iz}(\epsilon) = \frac{\sigma_0}{E_{iz}^2 x^{b_{iz}}} \left( \frac{a_{iz} x - a_{iz}}{a_{iz} x + 1} \right)^{c_{iz}}$$

where  $E_{iz} = 15.76$  eV is the threshold energy for the cross-section,  $x = \epsilon/E_{iz}$   $\epsilon$  is the electron energy, and  $\sigma_0 = 6.5 \times 10^{-17}$  m<sup>2</sup>,  $a_{iz} = 0.5$ ,  $b_{iz} = 0.87$ ,  $c_{iz} = 1.4$ .

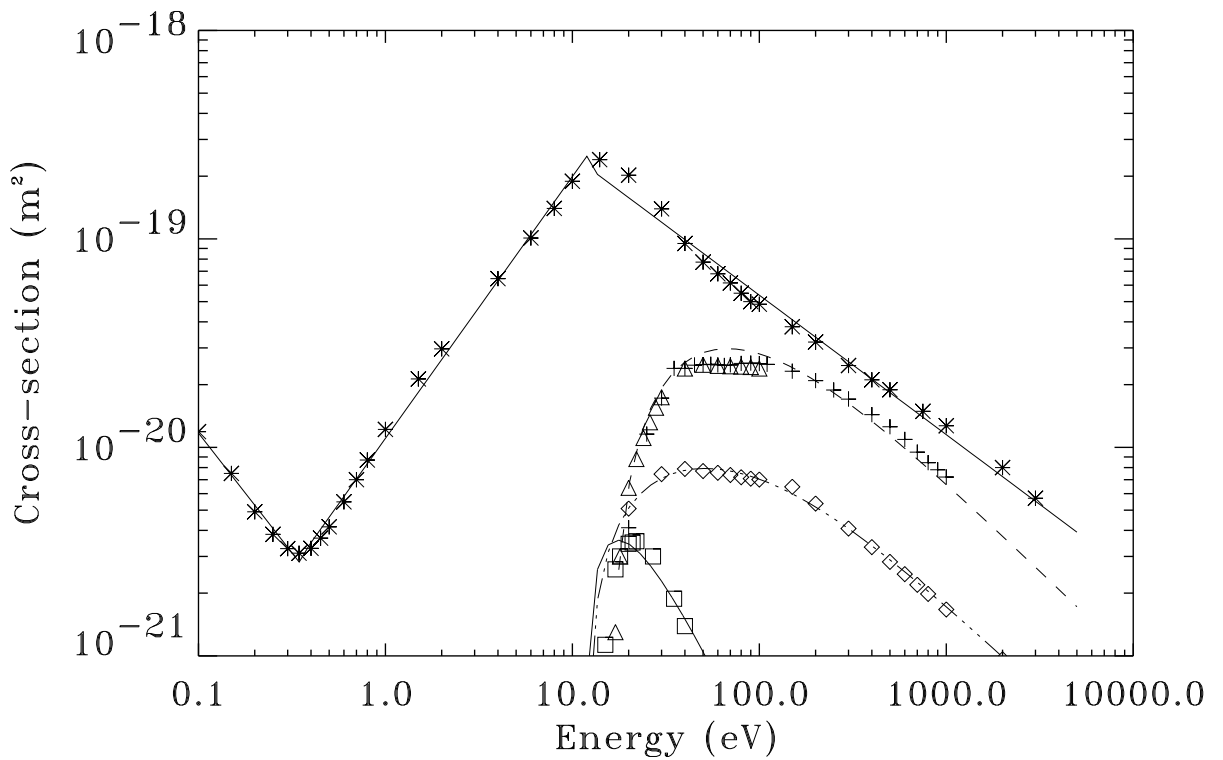


Figure 2: Electron-Argon cross-sections as a function of energy - solid lines are HBS curve fits and symbols experimental data: elastic cross-section data (asterix) 0 – 20 eV [10] and 20 – 3000 eV [6]; excitation to (lumped) radiative state (diamonds) [6] ; excitation to (lumped) metastable state (squares) [7]; single-step ionisation (triangles) [11] and crosses [8].

*Excitation to lumped radiative levels*

$$\sigma_{ex}(\epsilon) = \frac{\sigma_0}{E_{ex}^2 x^b} \frac{a_{ex}x - a_{ex}}{a_{ex}x + 1}$$

where  $E_{ex} = 11.62$  eV is the threshold energy for the cross-section,  $x = \epsilon/E_{ex}$  and the constants  $\sigma_0 = 1.1 \times 10^{-17}$  m<sup>2</sup>,  $a_{ex} = 0.18$ ,  $b_{ex} = 0.85$ .

*Excitation to lumped metastable levels*

$$\sigma_m(\epsilon) = \frac{\sigma_0}{E_m^2 x^b} \frac{a_m x - a_m}{a_m x + 1}$$

where  $E_m = 11.55$  eV is the threshold energy for the cross-section,  $x = \epsilon/E_m$  and the constants  $\sigma_0 = 3.5 \times 10^{-18}$  m<sup>2</sup>,  $a_m = 8.0$ ,  $b_{ex} = 2.0$ .

*Elastic scattering*

$$\begin{aligned} \sigma_{el}(\epsilon) &= 8.3 \times 10^{-22} \epsilon^{-1.15} & \epsilon \leq 0.345eV \\ &= 1.1 \times 10^{-20} \epsilon^{1.26} & 0.345eV > \epsilon > 12.0eV \\ &= 1.2 \times 10^{-18} \epsilon^{-0.67} & \epsilon \geq 12.0eV \end{aligned}$$

Electrons make anisotropic collisions, with the scattering angle chosen using [9]

$$\cos \theta = \frac{2 + \epsilon - 2(1 + \epsilon)^R}{\epsilon}$$

where  $R$  is a random number, uniformly distributed between 0 and 1.

### **LK Cross-sections**

The cross-section curve fits (shown in Figure 3) have the form

*Ionisation*

$$\sigma_{iz}(\epsilon) = 3.18 \times 10^{-20} \frac{\ln x}{x} \quad x > 1$$

where  $E_{iz} = 15.76$  eV is the threshold energy for the cross-section,  $x = \epsilon/E_{iz}$  and  $\epsilon$  is the electron energy.

*Excitation to lumped radiative levels*

$$\sigma_{ex}(\epsilon) = 1.56 \times 10^{-20} \frac{\ln x}{x} \quad x > 1$$

where  $E_{ex} = 11.62$  eV, is the excitation threshold energy and  $x = \frac{\epsilon}{E_{ex}}$ .

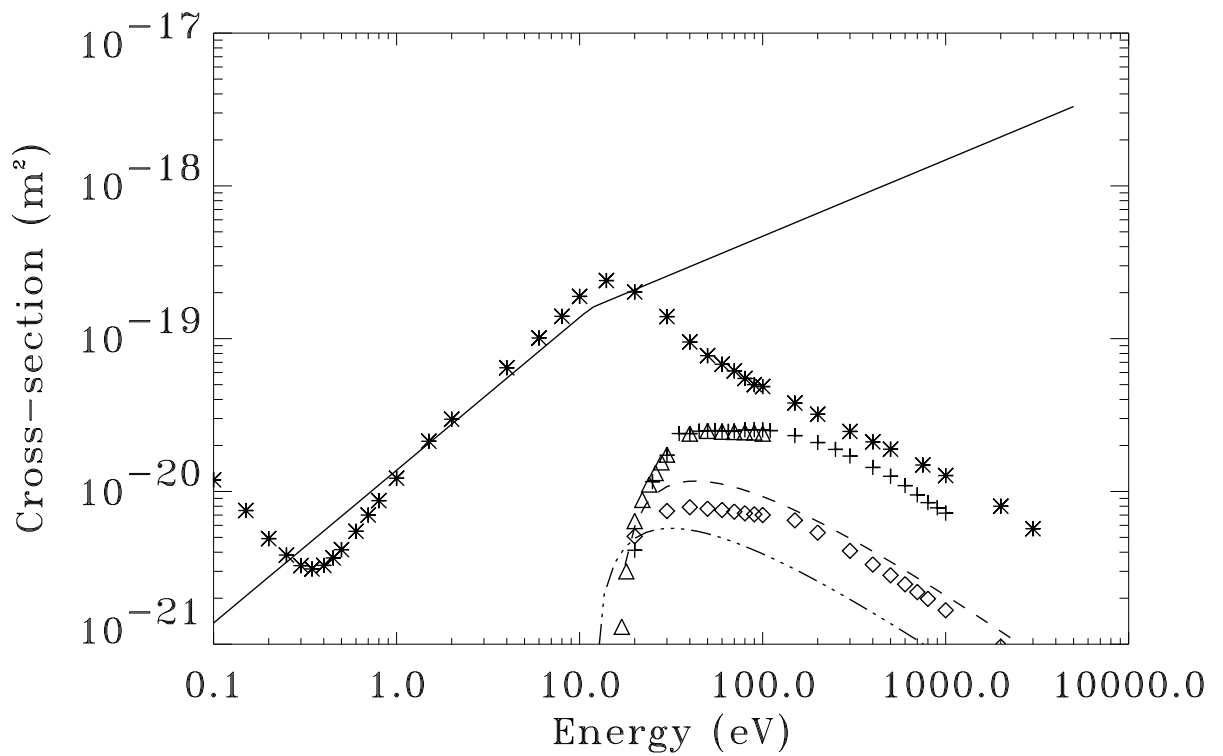


Figure 3: Electron-Argon cross-sections as a function of energy - solid lines are L&K curve fits and symbols experimental data: elastic cross-section data (asterix) 0 – 20 eV [10] and 20 – 3000 eV [6]; excitation to (lumped) radiative state (diamonds) [6]; single-step ionisation (triangles) [11] and crosses [8].

*Elastic scattering*

$$\begin{aligned}\sigma_{el}(\epsilon) &= 1.59 \times 10^{-19} \frac{\epsilon}{11.55} & \epsilon \leq 11.55eV \\ &= 1.59 \times 10^{-19} \sqrt{\frac{\epsilon}{11.55}} & \epsilon > 11.55eV\end{aligned}$$

Lawler and Kurtsgshagen do not determine a curve fit for the excitation to metastable state cross-section. They assume that the collision scattering angle is isotropic so that

$$\cos \theta = 1 - 2R$$

where  $R$  is a random number, uniformly distributed between 0 and 1.

#### 4.1.6 Ion-Neutral Cross-sections

The ion-neutral cross-section curve fits (shown in Figure 4) have the form

*Charge exchange*

$$\sigma_{ex} = (7.0 - 0.38 \ln \epsilon)^2 \times 10^{-20}$$

where  $\epsilon$  is the ion energy and  $\sigma_{ex}$  is in units of metres squared. This empirical form is found to be true over a wide energy range [15].

*Elastic scattering*

$$\sigma_{el} = (6.45 - 0.365 \ln \epsilon)^2 \times 10^{-20}$$

#### 4.1.7 Species Parameters

One set for each species should be specified.

max-np	The maximum number of particles per species.
q	Charge per physical particle [C].
m	Mass per physical particle [kg].
j0L	Magnitude of injected current density from the left electrode [Amps/m <sup>2</sup> ].
j0R	Magnitude of injected current density from the right electrode [Amps/m <sup>2</sup> ].

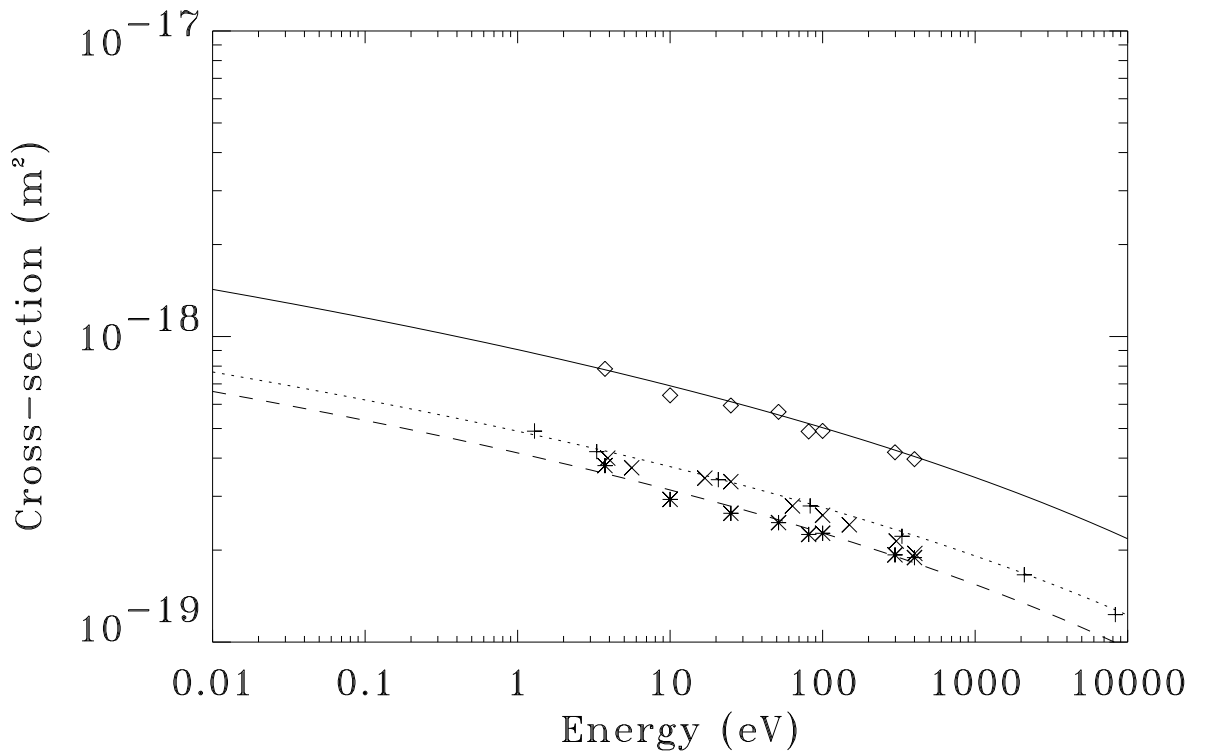


Figure 4: Argon ion-neutral cross-sections as a function of energy - solid lines are curve fits and symbols experimental data: elastic cross-section data (asterix) [13]; charge exchange (+) [13] and (x) [14]; total cross-section (triangles) [13].



initn	Initial species physical density in the system [ $\text{m}^{-3}$ ].
profile	Specifies initial profile when loading new discharge 1 - uniform profile 2 - bessell function profile 3 - cosine profile
sp_k	number of time-steps between each particle push, so the effective time-step for the species is sp_k.dt. Allows ions to be moved on longer time-scale than electrons.

#### 4.1.7.1 Velocity Distribution

vr_0L	Drift velocity for $v > 0$ particles [m/sec].
vr_0R	Drift velocity for $v < 0$ particles [m/sec].
vr_tL	Thermal velocity for $v > 0$ particles [m/sec].
vr_tR	Thermal velocity for $v < 0$ particles [m/sec].
vr_cL	Cutoff velocity for $v > 0$ thermal distribution [m/sec].
vr_cR	Cutoff velocity for $v < 0$ thermal distribution [m/sec].
v0t	Drift velocity in the theta directions for particles [m/sec].
vtt	Thermal velocity in the theta direction for particles [m/sec].
v0z	Drift velocity in the z direction for particles [m/sec].

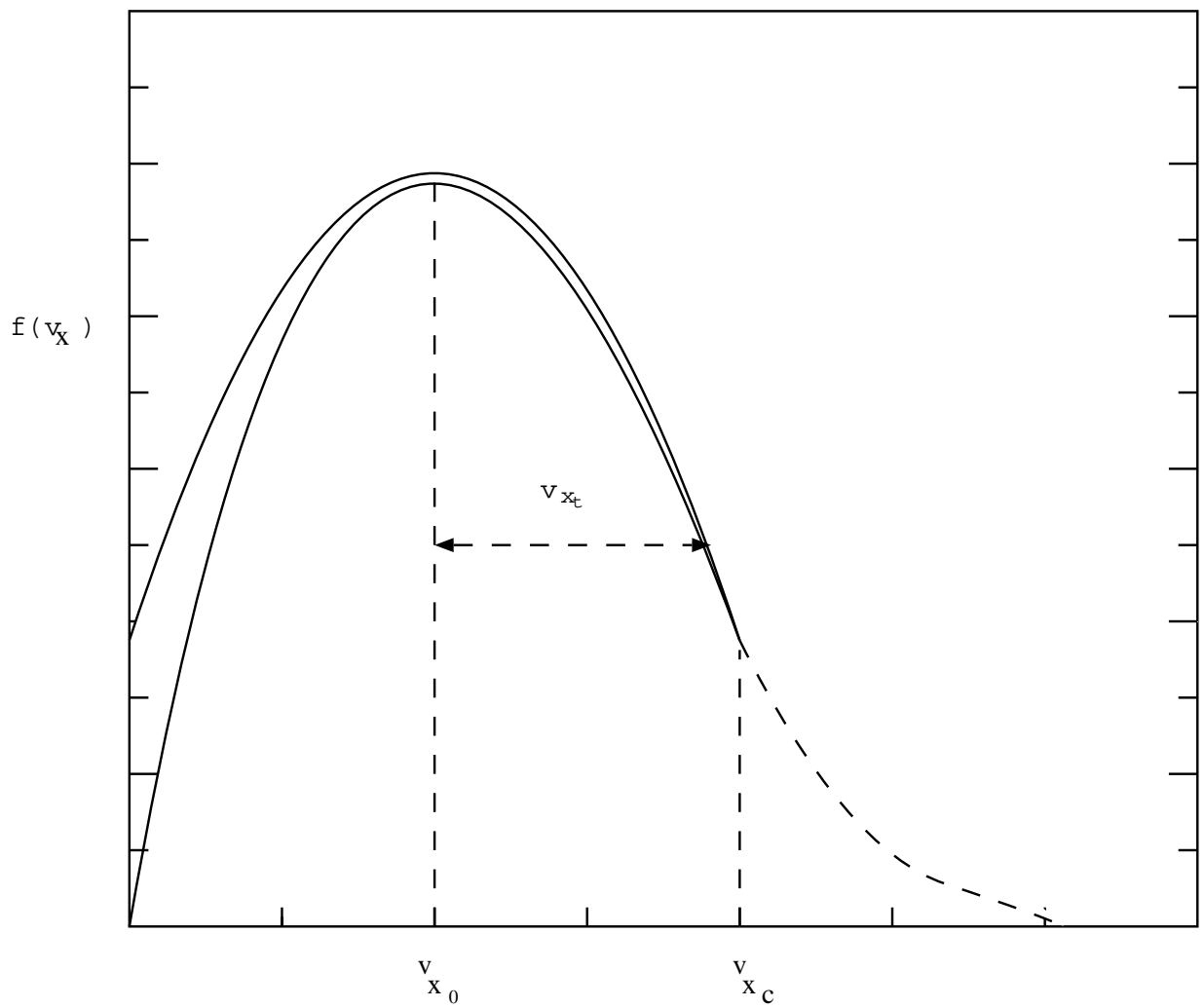


Figure 5: Velocity distribution function in x-direction. The distribution function in the perpendicular direction does not have a cutoff, but may have a drift.

vtz            Thermal velocity in the z direction for particles [m/sec].

#### 4.1.7.2 Energy Distribution Diagnostics

This line determines the parameters for the energy distribution function at the electrode(s).

nbin        Number of bins for the energy distribution diagnostic of the species at left wall.

Emin        The minimum energy seen in the energy distribution diagnostic of the species at left wall [eV].

Emax        The maximum energy seen in the energy distribution diagnostic of the species at left wall [eV].

max-np     The maximum number of particles per species.

Parameters for an energy distribution function within the discharge. The parameters XStart and XFinish designate a region (a window) in the space over which the energy distribution is calculated.

nbin        Number of bins for the energy distribution diagnostic of the species in the system.

Emin        The minimum energy seen in the energy distribution diagnostic of the species in the system [eV].

Emax        The maximum energy seen in the energy distribution diagnostic of the species in the system [eV].

- XStart        The left boundary of the region over which the distribution is calculated.
- XFinish       The right boundary of the region over which the distribution is calculated.

### 4.1.7.3 Velocity Distribution Diagnostics

These parameters specify parameters for the velocity distribution function as a function of position, for each velocity component. Note that this diagnostic is expensive both in memory and run-time, so it is only calculated if  $nbin > 0$ .

- vx\_lower       Lower velocity for velocity distribution diagnostics [m/sec].
- vx\_upper       Upper velocity for velocity distribution diagnostics [m/sec].
- nxbin         Number of bins used. (if 0 diagnostics is turned off.)
- vy\_lower       Lower velocity for velocity distribution diagnostics [m/sec].
- vy\_upper       Upper velocity for velocity distribution diagnostics [m/sec].
- nybin         Number of bins used. (if 0 diagnostics is turned off.)
- vz\_lower       Lower velocity for velocity distribution diagnostics [m/sec].
- vz\_upper       Upper velocity for velocity distribution diagnostics [m/sec].
- nzbin         Number of bins used. (if 0 diagnostics is turned off.)

## 4.2 Radiation transport Parameters

These parameters specify the physical and numerical parameters of the considered resonant species.

nc	The number of spatial cells for the radiation transport routine. The number of PIC simulation cells should be a multiple of it.
Lambda	The wavelength of the considered resonant emission [nm].
line_shape	The type of lineshape. The Doppler (D), and the Lorentz (L) lineshapes are installed but the Voigt (V) lineshape is not prepared yet.
A_ki	Einstein coefficient of the transition from the excited state to the ground state [ $10^8$ /sec].
k0	The absorption coefficient at the line center. This value is calculated automatically from other simulation parameters such as gas pressure, A_ki, and lineshape, but it is also possible to use arbitrary value. Be sure to compare the value in the input file with the value calculated by the code.
sp_k	Number of time step of radiation transport routine is $sp\_k \times dt$ .
x_min[max]	The lower[upper] limit of the frequency domain. This value should be large enough to be able to neglect the truncation error. Users should be careful for the Lorentz lineshape which has long tails.
x_bin	Number of bins used in the frequency domain.

## References

- [1] C. K. Birdsall and A. B. Langdon, *Plasma Physics Via Computer Simulation*, (McGraw-Hill 1985, Adam-Hilger 1991 which has ES1 disk).
- [2] R. W. Hockney and J. W. Eastwood, *Computer Simulation Using Particles*, Adam Hilger (1988).
- [3] W. S. Lawson, *PDW1 User's Manual*, Electronics Research Laboratory Report M84/37 (1984).
- [4] J. P. Verboncoeur and V. Vahedi, *WinGraphics: An Optimized Windowing Environment for Plasma Simulation*, Proceedings of 13<sup>th</sup> Numerical Simulation Conference, Sante Fe, NM (1989).
- [5] John P. Verboncoeur, M. Virginia Alves, V. Vahedi, and C. K. Birdsall, *J. Comp. Phys.* **104**, 321 (1993).
- [6] F.J. deHeer, R.H. Jansen and W. van der Kaay, C. K. Birdsall, *J. Phys. B* **12**, 979 (1979).
- [7] D.H. Madison, C.M. Maloney, J.B. Wang, *J. Phys. B* **31**, 873 (1998).
- [8] E. Krishnakumar and S.K. Srivastava, *J. Phys. B* **21**, 1005 (1988).
- [9] V. Vahedi and M. Surrendra, *Computer Physics Communications* **87**, 179 (1994).
- [10] J. Ferch, B. Granitza, C. Masche and W. Raith, *J. Phys. B* **18**, 967 (1985).
- [11] Viktor, *Fizika* **21**, 345 (1989).
- [12] U. Kortshagen and J.E. Lawler *J. Phys D: Appl Phys* **32**, pp 3188-3198 (1999)
- [13] E.W. McDaniel, "Collision Phenomena in Ionised Gases", John Wiley & Sons, New York (1964).
- [14] D. Rapp and W.E. Francis, *J. Chem. Phys.* **37**, 2631 (1962).
- [15] E.A. Mason and E.W. McDaniel, "Transport Properties of Ions in Gases", John Wiley & Sons, New York (1988).